Flow Simulation over a Glider

CFD Study with Transition SST and k-ω SST turbulence models in Fluent

Jose Luis González García (josgo473)

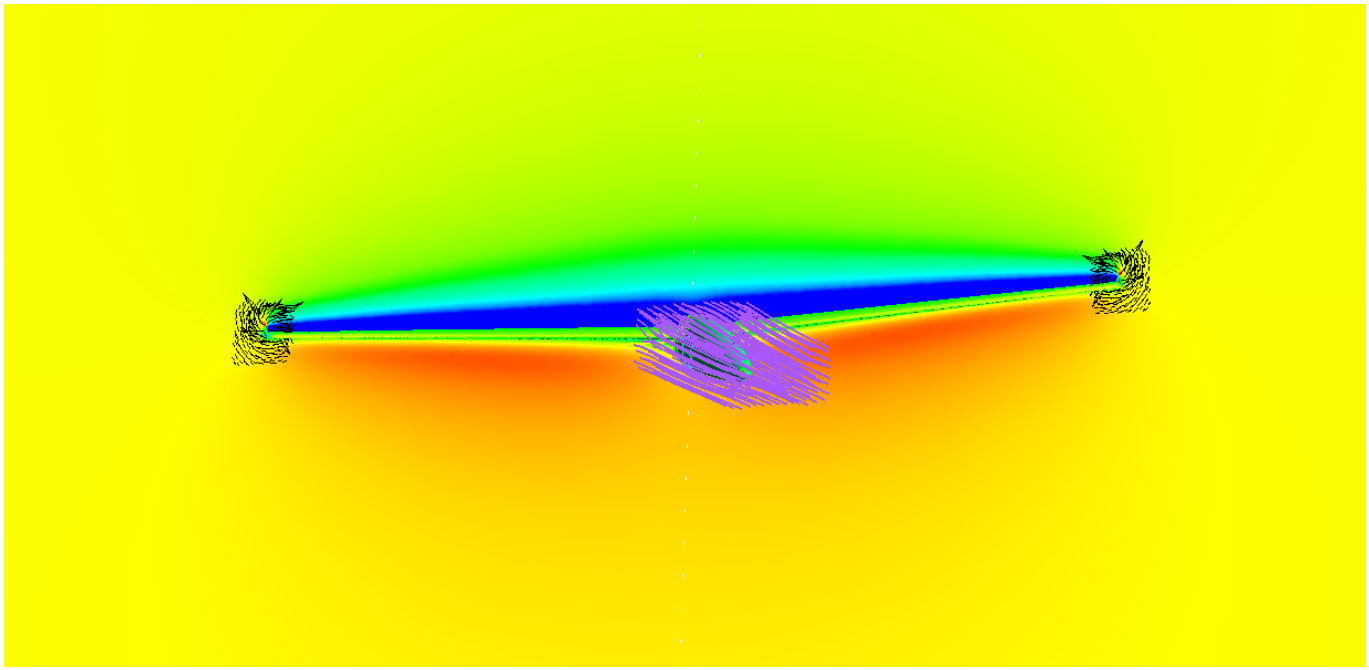

Linköpings universitet
Institutionen för ekonomisk och industriell utveckling
Examensarbete 2019|LIU-IEI-TEK-G–19/01694âSE

Linköpings universitet
Institutionen för ekonomisk och industriell utveckling
Ämnesområdet Mekanisk värmeteori och strömningslära
Examensarbete 2019|LIU-IEI-TEK-G–19/01694âSE

Flow Simulation over a Glider

CFD Study with Transition SST and k-ω SST turbulence models

Jose Luis González García (josgo473)

Academic supervisor: Roland Gårdhagen
Examiner: Hossein Nadali Najafabadi

Linköping universitet
SE-581 83 Linköping, Sverige
013-28 10 00, www.liu.se

Abstract

CFD has become one of the mos important engineering tools in order to understand the fluid mechanics of a problem in a cheaper and less complicated way than the experimental methods previously used. Even though it is not a perfect tool, it has been proved as a very useful way of problem approaching and solving. One of the most important aspects related to CFD is that it comes from numerical methods, so it has a determined level of uncertainty and it has to be validated with real or experimental data in order to check that the results are feasible and correct. The Reynolds Averaged Navier-Stokes (RANS) methods which model all the turbulence in the simulation must be checked even more due to its nature of modelling what is happening. In this assignment CFD is used in order to simulate the flow around a glider, more exactly the Standard Cirrus Glider which is a sailplane built by the Company Schemp-Hirt during the seventies and eighties. In this thesis two different turbulence models are used which are Transition SST ($\gamma - Re_\theta$) and the well-known k-ω SST together with the results of the thesis performed by Thomas Hansen [1] in order to verify the method and validate the results. Data from the NASA [2], the software XFOIL and the experimental in flight measurements of IDAFLIEG [3] is also used in this purpose.

The Transition SST model has been proved as the model which better adapts to the reality which has been chosen for the 3D analysis due to its much better performance in capturing reality. The 3D analysis revealed that the best glide ratio obtained in the range of speed analyzed ([90,95,100] [kmh]) has been found in 100 [kmh] with a value of 34.94 underestimating the experimental value of 36.5. The estimated Oswald factor obtained from the calculations has been 0.78. The addition of a winglet in the wing tip has reported an average of 1.5% of Drag reduction.

Acknowledgements

The work presented in this report has been done from February to June in 2019, far away from the sunny Mediterranean coast where I started my journey in the Engineering World. The opportunity which was given to me when I was given this Erasmus Scholarship has changed my life in every aspect and has given me the opportunity to grow as a person and as an engineerg.
It is mandatory to express my gratitude to everyone of those people that have made this Final Bachelors Thesis possible. First of all, thanks to my supervisor Roland Gårdhagen for giving me this opportunity and for the help provided in every step and critical moment. Thanks to Linköping Univeristy for providing the facilities used in this project. Thanks to my Erasmus fellows which have made a home from Linköping, specially to Luis García, Cesar Jiménez, Guillermo Puelles, Teresa Aparicio and Carmen Velasco for those uncountable hours spent in the Laboratory and for the support in the difficult times. And last but not least, thanks to my family, for showing me that hard work and determination are the features that make the difference.

Nomenclature

Abbreviations and Acronyms

Abbreviation	Meaning
LiU	Linköping University
CFD	Computational fluid dynamics
CAD	Computer aided design

Fluid Mechanics and Turbulence

Symbol	Description	Units
A	area	$[m^2]$
TKE	Turbulent Kinetic Energy	$[J/kg]$
ϵ	Turbulent Dissipation Rate	$[m^2/s^3]$
ω	Specific Dissipation Rate	$[1/s]$
t	Time	$[s]$
V	Velocity	[m/s] or [kmh]
μ	Dynamics viscosity	$[kgm^{-1}s^{-1}]$
ρ	Density	[kg/m^3]
L	Length	[m]
R	Ideal Gas Constant	$[Jkg{-}1Kk{-}1]$
q	Dynamic Pressure	[Pa]
P	Pressure	[Pa]
u, v, w	Velocity Components	[m/s]

Aerodynamics

Symbol	Description	Units
a.o.a.	Angle of attack	$[deg]$
C_F	Force coefficient (lift or drag)	$[-]$
AE	Aerodynamic Efficiency	[-]
CP	Pressure Coefficient	[-]
b	Wingspan	[-]
AR	Aspect Ratio	[-]
M	Mach number	[-]
h	Sink Rate	[m/s]
GR	Glide Ratio	[-]
ϕ	Gliding Angle	[-]

Subscripts and superscripts

Abbreviation	**Meaning**
i	Induced (Drag)
0	Parasitic (Drag)
∞	freestream condition
’	Instantaneous variable (Turbulence)

Contents

1 Introduction

Fluid mechanics inner complexity stems from the difficulty that arises when describing the physics behind this field; mainly ruled by the governing equations of the Fluid Dynamics, which are the Mass , Momentum and energy equations. These equations are partial derivative equations which cannot be solved analytically. That is why the Numerical Methods are extremely important in Fluid Dynamics, because nowadays there are the only way to solve the governing equations in an accurate way for complex problems. Those numerical methods were performed by hand in the yesteryear, but since the apparition of CFD codes, which were able to solve this numerical methods with an accuracy unseen before. Since the 1950's the CFD codes were able to be used in 3D calculations, but only for research purposes due to the huge computational cost that was required and thus the great time that had to be spent even in simple cases. After the exponential increase in computational power which happened in the last decades of the 20th century CFD codes became finally a good alternative to the wind tunnels and the rest of experimental methods in Aerodynamics[4]. From that date onwards, new codes and companies started using this computational method and nowadays there are different types of codes developed by many companies such as Star CCM+, ANSYS, Open Foam, and many other open source codes more focused in research due to the lack of constrictions in those type of codes. It can be said that the main software used nowadays for industrial CFD applications is ANSYS (FLUENT or CFX), being ANSYS FLUENT the one used in this Project and STAR CCM+ which was the one used by Thomas Hansen on his research [1]. In this project two different models have been used in order to approach the study in the more realistic way considering the RANS method possibilities. Two models have been implemented in the project, which are the $k-\omega$ SST and the Transition SST ($\gamma-Re_\theta$), which will be shortly described in this section.

The gliders are general aviation aircraft which are well known because of its great aerodynamics. Gliders have been around for a long time and they have been defined by its no engine flight, which is the reason of their good design trying to increase the in flight time. Standard Cirrus Glider was introduced in the sixties and even today it is a glider of an incredible quality. The Schemp-Hirt Company has been updating and adapting it to the new times in order to take advance of its good design.

The aim of this project is to perform an analysis of the gliding performance of the Standard Cirrus Glider and analyze the effect of the addition of winglets in the original geometry. In order to do so, the project has been divided into two parts, one studying and choosing the turbulent models in 2D and the one which actually studies the glider and performs the glider study.

1.1 2D Study

The first part of this thesis addresses the study of the airfoil which is used in the Standard Cirrus Glider wing outer section, which is the airfoil FX 66-17 A II-182.

The main objective of this part is to compare the behavior between two turbulence models used in Fluent, K-ω SST and Transition SST γ-Re_θ with the results obtained by Tomas Hansen in his study [1] and also with the different NASA studies and with other software like Xfoil. The objective of this part is to validate the method followed in order to be able to apply it in the next steps of the project. The second aim is to understand how the turbulent models behave in order to choose the most accurate one in the subsequent 3D studies as well as obtaining a full understanding of the flow around the previously mentioned airfoil.

1.2 3D study

Once a correct methodology has been established and the turbulent model has been chosen, it is time to simulate the whole Standard Cirrus Glider geometry. This will allow to understand the flow around the glider and also to know where the most determinant features are, which is crucial to be able to modify the geometry afterwards and improve the glider performance. In addition, it is necessary to find the steady flight conditions for the speeds evaluated in order to obtain the conditions to compare the performance with experimental in-flight measurements which where done in IDAFLIEG[3], where the Standard Cirrus Glider was studied and evaluated. CFD gives the possibility to obtain different values in different conditions of flight, and this study is going to take advantage of that in order to be able to calculate the Oswald factor of the aircraft by means of different types of simulations. Once the former aims have been achieved, the last part of the study will be shown, which is the evaluation of the addition of a Winglet and the repercussions it has on the flow field and the generation of Aerodynamic forces.

1.3 Standard Cirrus Glider

The Standard Cirrus Glider is an aircraft designed in the 1960s by the Engineer Klaus Holighaus, one of the best well known glider builders at the Schempp-Hirth factory, in Kirchheim (Germany). Her first flight was performed in 1969 and it was produced between 1969 and 1985, being updated with later modifications in order to increase its already good flying and gliding performance. About 850 Standard Cirrus Gliders were built, 75 of which were not built in Schemp-Hirth factory in Germany, but built by licence in Yugoslavia (nowadays Serbia) at the Vazduhoplovno Tehnicki Centar.

The Standard Cirrus Glider is a one-manned high-wing aircraft with 15 [m] of wingspan and T-tail configuration. the wing is built with a 3 [deg] dihedral and a 2 [deg] sweep angle in the leading edge combined with a 3 [deg] sweep angle in the trailing edge. Everything combined makes an Aspect Ratio of 22.5. The length of the fuselage is 6.35 [m] and its height is 1.32 [m] combined with a take off weight of 355.6 [kg]. It is a glider with retractable landing gear. The wings are designed with geometrical twist, which means that the airfoils change along the wingspan in order to obtain better maneuverability, preventing some parts of the wing from getting stalled before others. The root airfoil is the FX S 02-196 and the outer section main airfoil is the FX 66-17 A II-182. The main features of the aircraft geometry are depicted in figure 1.

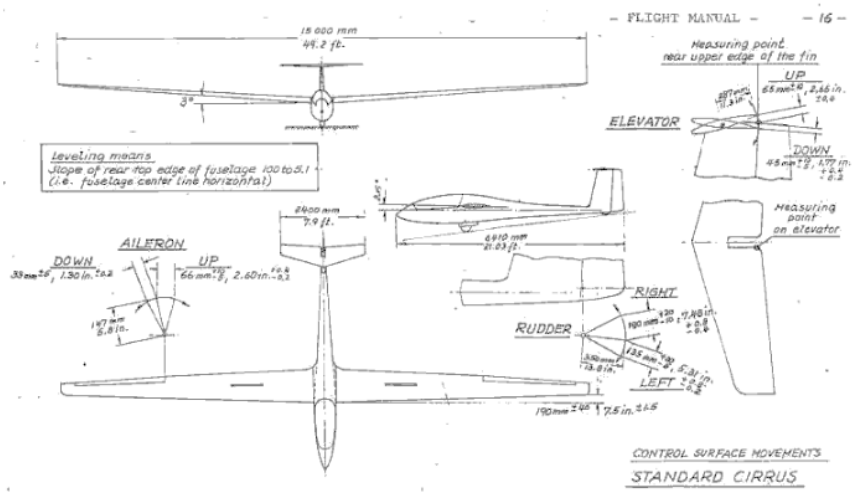

Figure 1: Standard Cirrus Glider main geometry features [5]

Some other features of the Standard Cirrus Glider are performance-related given by The builder Schempp-Hirth gives the values from their calculations from experimental measures and these are presented in table 6:

Performance Data	
Min Sink	0.6 [m/s]
Best Glide Ratio	36.51 [-]
V_{Stall}	62 [kmh]
V_{NE}	220 [kmh]

Table 5: Performance Data of the Standard Cirrus Glider

Main Features	
Wing Configuration	Mid Wing
Tail Configuration	T Tail
Landing Gear	Retractable
Crew	1
Weight	355.6 [kg]
V_{Stall}	62 [kmh]
V_{NE}	220 [kmh]
Best Glide Ratio	36.51 [-]

Table 6: Performance Data of the Standard Cirrus Glider

2 Fluid Mechanics Background

Fluid mechanics is a complex field, and in order to make the understanding of the project easier for the reader, some basic background is given in this section.

2.1 Turbulence and Transition

When it comes to talk about the Turbulent Transition, the first step is to set the background of the two different types of flow. These are laminar and turbulent flow, but even before, it is of utmost importance to describe the main adimensional number that sets in which of those flows a fluid is in a particular situation. This number is the Reynolds number, an adimensional number which expresses the relation between the inertial and viscous forces exerted in a fluid. It is a macroscopic parameter which can be expressed globally in a flow or also locally expressing the features of the flow in a certain region. The Reynolds number is expressed in equation 1.

$$Re = \frac{\rho_\infty V_\infty L}{\mu_\infty} \tag{1}$$

Being ρ the density of the freestream flow, V the velocity of the freestream flow, L the characteristic length, which vary on each problem, i.e. the chord of the airfoil in the 2D part or the length of the aircraft in the 3D part, and finally the dynamic viscosity of the freestream flow.

There is not a Reynolds number that produces the turbulent transition but instead, depending on the type of problem, the critical Reynolds number varies depending on the features of the flow (internal, external, geometry, ...).

Laminar flow is characterized by the smooth movement of the fluid particles creating parallel layers of fluid which are not perturbed and with low molecular and velocity mixing. On the other hand, the turbulent flow is featured by an unsteady behavior of the particles enhancing the molecular and velocity mixing creating infinitesimal vortex and bigger structures which make the study of the flow incredibly difficult to handle. One of the main differences of both flows occurs in the Boundary Layer, which is the region of a fluid that varies its velocity from 0 to 99% of the freestream velocity when the fluid is in contact with a surface, given that the null velocity is located in the zone attached to the wall. Both Turbulent and Laminar Boundary Layers are quite different and so are their effects in the flow. It is interesting to mention that due to the shear stress which happens between the surface and the fluid (due to the non slip condition in of the viscous flow) and also due to the adverse pressure gradients generated in an airfoil due to the velocity changes along its chord, sometimes, the flow looses its velocity and arrives to what is called the stagnation point inside the Boundary Layer, creating in that way a "separation bubble" where the Boundary Layer is detached. This phenomena is closely related to laminar flow and usually when the flow becomes turbulent is reattached because

of the greater energy of this type of flow [6] .

As mentioned before, Reynolds number can be used to describe local conditions and due to this fact, it is possible to estimate the state of the fluid on each location, using the local variables instead of the freestream variables. Following this reasoning and considering that the Reynolds number is an indicator of the type of flow that the fluid is developing, it is very interesting to use it to evaluate whether the flow is developing a Laminar or a Turbulent flow and when it changes. In light of this idea, it is mandatory to mention that a flow in contact with a surface starts being Laminar by default, and when the flow reaches the Transition Reynolds number (both by reaching a given distance or by increasing a certain velocity which makes the Reynolds number to achieve the Transition value) it starts the Turbulent Transition behaving in between those two states of the fluid and going towards the turbulent behavior as it is depicted in figure 2.

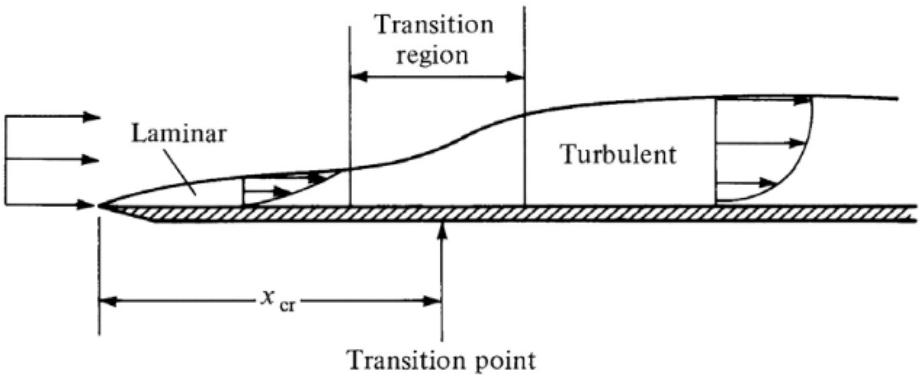

Figure 2: Flow over a flat plate [7]

The transition point has usually been a difficult field for the RANS CFD simulations, because of the difficulty of the turbulent handling and that is why the Transition SST ($\gamma - Re_\theta$) turbulent model has popped up as a good way to obtain better results lately.

2.2 Turbulent Models

Due to the intrinsic complexity of the Turbulent Flow, it has been challenging to adapt a numerical method as the CFD to the non-repeatable, instantaneous and chaotic nature of the Turbulent Flow [8]. In order to achieve good quality simulations in the Turbulent Field enhancing the use of CFD in the industry, some improvements were done in the CFD codes, such as FLUENT, introducing equations to the four initial governing equations in order to be able to predict the turbulent effects [9]. The basic Turbulence treatment and the one widely used in industry due to its quality vs computational cost relation is RANS (Reynolds-Average Navier Stokes), which does not simulate the turbulence but models it in both, the bigger and smaller scales of turbulence. There are models inside the RANS spectrum with one additional equation like Spalart Allmaras, and others more advanced with two equations like $k-\omega$ and $k-\epsilon$. Nowadays, there are models with even four additional equations, as the Transition SST, which can predict the behavior of a flow with greater accuracy.

2.2.1 $k-\omega$ SST Model

Given the characteristics of the models $k-\omega$ and $k-\epsilon$, the SST was created by Enter Menter [10] in order to merge the strengths of those two models taking into advance the good behavior of the $k-\epsilon$ in the freestream flow, inducing good results when applied outside the boundary layer, and the features of the $k-\omega$ when it is close to a wall inside the Boundary Layer. The key for understanding the behavior of SST is in the two equations which add to the governing equations. The SST model uses the k equation of $k-\omega$ model and rewrites the ω equation of the $k-\omega$ model but replacing the ω by the equation shown in 2.

$$\omega = k * \epsilon \tag{2}$$

In this way, both models are blended in a way that givesthe new model the benefits from the $k-\omega$ in the freestream and from the $k-\epsilon$ close to the wall.

The mesh requirements for this turbulent model is to use a Y+ of 1 in order to do a proper Boundary Layer treatment.

2.2.2 Transition SST ($\gamma - Re_\theta$)

Turbulent transition [11] models are an improvement in the use of CFD codes in general aerodynamics mainly in the cases which require an accurate prediction of the interaction in the Boundary Layer. These types of models allow the combination of correlation based transition models and the usual Turbulent models used in CFD.

Transition models are original approaches to the problems avoiding non-local information in correlation based models. The aim of this models is to avoid the deficiencies of the original turbulent formulation and calibrate a larger spectrum of flux conditions.

The new formulation uses 2 transport equations, which are the intermittency used to start the transition process and an equation formulated to avoid non local operations introduced by quantities used in experimental correlations such as the γRe_θ.

The second equation, in this case, is the equation for the local momentum thickness of the Reynolds number, which is used to initiate the transition with the local conditions.

The mesh requirements for this method are a high quality refined mesh in the Boundary Layer, which must achieve Y+ values between 0.1 and 1 in order to be able to obtain the transition process.

2.3 Aerodynamic Forces

When a body is immersed in a moving flow (whether the source of the movement is the body or the fluid does not matter) the interactions between the body and the fluid generate several phenomena. It is known that the interaction between the fluid and the body creates certain forces. The explanation for those forces become trivial for the 2D spectrum and any reference needed to the 3D spectrum will be done, but the reader should consider a 2D space to obtain a full understanding about the nature of these forces [12] where the fluid is moving in the X direction.

Lift Force

The Lift force is the force that appears in the body in the direction perpendicular to the fluid movement, it is formed mainly by the pressure differences between the upper and lower surfaces and also in an small part by the integration of Y of the shear stresses in the Y direction, which can be positive or negative to the addition of the pressure forces.

Drag Force

The Drag force is the force that appears in the body in a direction parallel to the fluid movement and it creates resistance to the movement of the body through the fluid, in other words, it pushes the body in the direction in which the fluid is moving. Drag force has different components, which in 2D are just friction force, considering Wall Shear Stress in the X direction and the action of the pressure field in the X direction, which is pressure drag. In 3D another component of Drag materializes, which is the induced drag. Induced drag is the drag created by the differences of pressure created by a finite 3D geometry which creates lift. This pressure difference materializes into a Wing Tip vortex which creates the induced drag, apart from reducing the amount of lift that the surface can create due to the downwash effect reducing the effective angle of attack of the wing. This makes easier the introduction of a zero lift drag, which is called the parasitic drag. The Parasitic Drag is composed by the friction drag and the pressure drag in the aircraft for the zero lift condition whereas the induced drag is only composed by drag created by the Wing Tip Vortex. Then the Drag force is represented by equation 3:

$$Drag = D_0 + D_i \tag{3}$$

3 2D Study: Airfoil Analysis

3.1 Method

The method of a CFD study is incredibly important as it is in any other experimental science, because it is what ensures a good correlation between the reality and the simulations performed. The method followed has been proved to be robust and it is mainly based in the one described in the Fluid Mechanics Extension Course of the Polytechnic University of Valencia [8].

3.1.1 Geometry

In external aerodynamics, the procedure for obtaining the domain which is going to be studied is somehow similar to the ones applied in the construction of a mold for casting. The body is subtracted of a bigger body and in that way, the fluid control volume is obtained. In this part of the project the airfoil geometry has been obtained from the web Airfoil Tools [13] in order to get a faithful representation of the Glider outer wing airfoil which is the FX 66-17 A II-182 represented in fig 3. All the modifications which were needed to obtain the control volume in order to perform the simulations were performed by means of the Design Modeller of ANSYS Workbench 19.2. The first step was importing the airfoil geometry to the software and then closing the airfoil surface, due to the gap generated in the trailing edge of the airfoil in Airfoil Tools. After that the Control Volume was created with the idea of preparing a good background for the future C-mesh. The idea is creating a Control Volume which consists on half a circle surrounding the leading edge joined with a rectangle in the trailing edge.

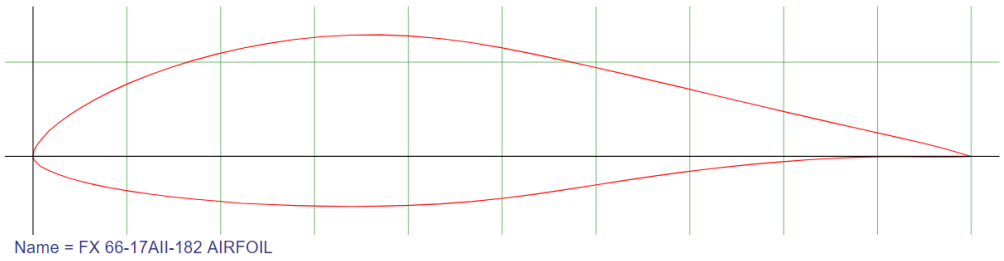

Figure 3: Airfoil FX 66-17 A II-182 obtained from [13]

The Control Volume domain was set following guidelines from [8] which states that the control volume must be at least 5 chords upstream and 20 chords downstream. In this thesis, the half circle has a radius of 6 chords and the rectangle has a length of 21 chords in order to cover the whole airfoil surface. The control volume for the airfoil at 0 [deg] of angle of attack is shown in figure with a chord of 0.458 [m] 4.

The geometry depicted in 4 was set as the base case for the rest of the angles of attack needed for the study, which correspond from -4 [deg] to 10 [deg] being allowed

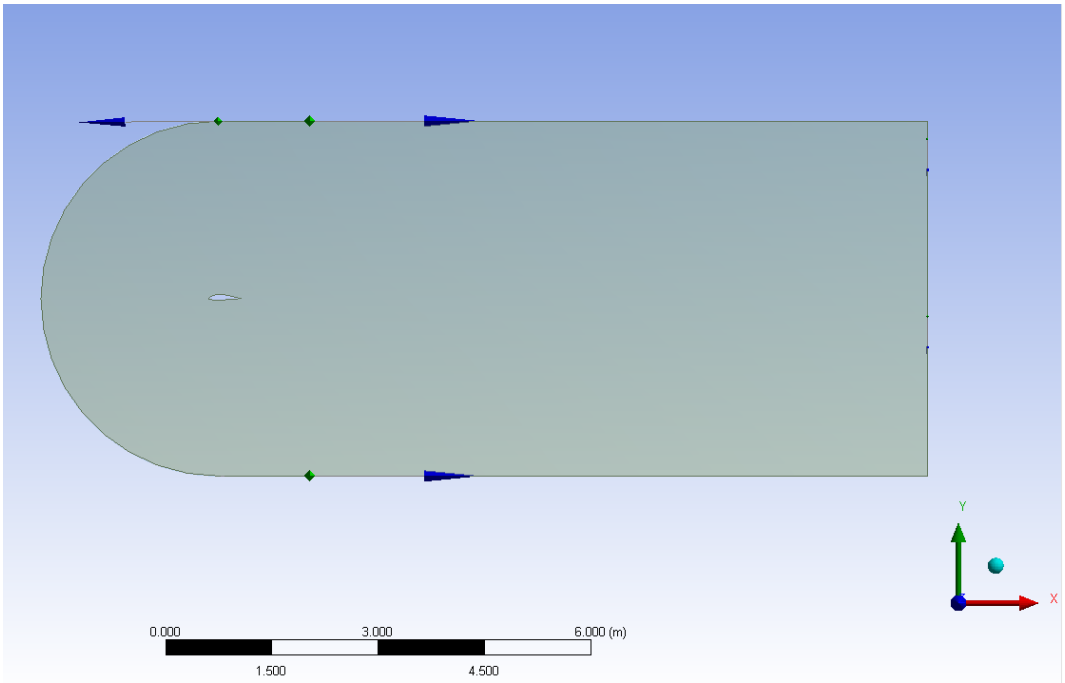

Figure 4: Control Volume for 0 deg angle of attack.

in this way to study the typical situations of the Lift coefficient vs angle of attack graph for this type of aircraft.

In order to achieve the desired angles of attack there are two possibilities, rotating the control volume or rotating the airfoil surface before doing the Boolean which leads to the final control volume. In this project the second option has been chosen due to the greater simplicity in the solver set up. In this way the Solver settings will be the same in all the cases.

3.1.2 Mesh

The 2D mesh is a structured 2D mesh formed by quads and directed by the user. In order to achieve an structured mapped mesh, quad elements have been chosen. This is because of their better performance for building an structured mesh and also due to the features of the flow, being a low speed aerodynamic profile, the flow is going to be mainly aligned with the quad mesh, enhancing the convergence and a better accuracy in the results. In Thomas Hansen study the mesh elected was a O-mesh type, but in this case the election has been a C-mesh due to the better performance of this types of mesh with regards to the wake of the airfoil. The number of elements used in the mesh around the airfoil has been kept as a constant following [1] with 600 elements around the airfoil. By means of a bias factor chosen in the building process of the mesh, the mesh has achieved a Y+ around 1 in order to be able to use the Near Wall approach by means of the number of elements in the Y-axis and a bias factor suitable for the Boundary Layer Treatment. In order to accomplish a mesh with the best accuracy/computational cost ratio, the verification study has

been performed in the 10 [deg] case for the Transition SST $\gamma - Re_\theta$ model, and the mesh set up has been exported to the rest of the cases. The mesh used in the 0 case deg after the mesh independence study is depicted in fig 5:

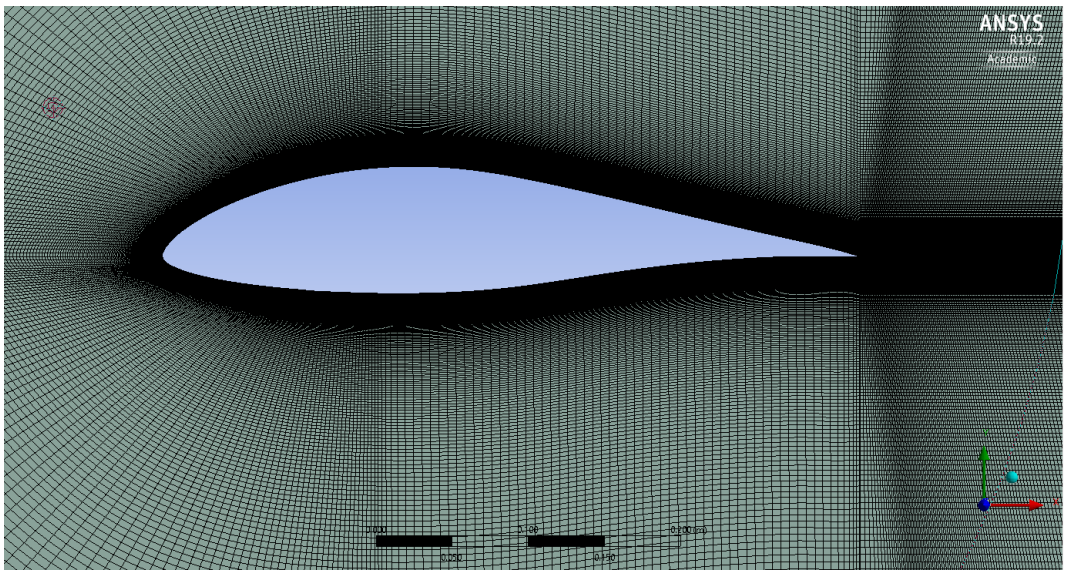

Figure 5: Mesh detail of the airfoil for 0 [deg] a.o.a.

In order to get the mesh independence and achieve a mesh which satisfies the conditions required for the accuracy of the problem. In this regard three different meshes have been analyzed in order to obtain the mesh independence and the information is contained in table 7:

Variables	**Coarse**	**Medium**	**Diff**	**Fine**	**Diff**
Elements	212925	505438	-	892903	-
Lift Coefficient	1.43	1.48	3.49%	1.47	0.54%
Drag Coefficient	1.83E-02	1.79E-02	2.16%	1.79E-02	0.00%
Max speed [m/s]	96.32	97.23	0.94%	96.81	0,43%

Table 7: Mesh independence study for the 10 [deg] of a.o.a.

The method followed to accomplish the mesh independence was increasing the number of elements in each dimension by 1.5 [8] and the criteria adopted to consider independent a mesh was to have an enough low value of averaged error (the mean of the relative error between the variables analyzed), which happens between the medium and the fine mesh with a 0.32% of difference. This was considered a good enough difference in order to achieve good results with the minimum computational cost possible, which is the main idea of the mesh independence study. Thus, the medium mesh settings are used in the whole spectrum of angles of attack.

It is mandatory to mention that in order to achieve the desired Y+ values, a preliminary study was performed using the flat plate approach for to obtain the wall shear stress and once done, using the Y+ expressions 4 it was possible to obtain the Y+ target. The values around the airfoil were in the range of 0.1 to 0.9. It was possible with the Bias factor of 50 in the mesh lines, which get a growth ratio approximately of 1.1.

$$Y+ = \frac{y\mu_\tau}{\nu} \tag{4}$$

3.1.3 Solver

In the solver settings, three different fields can be distinguished, they are the Boundary conditions, the schemes and models used, and the convergence criteria used in the problem.

First of all the meaning of Boundary Conditions (BC) must be explained. BC can be explained as the physical features which define the problem, and they are expressed as mathematical expressions of the assumptions which help to define the problem to be simulated. The BC location used in this project are depicted in figure 4. BC were established in table 8:

Inlet	A constant velocity inlet directed by a vector in the X direction and given by V in equation 6
Outlet	An static pressure outlet with the absolute pressure set to 1 atm in order to represent the absence of perturbation in the outlet
Free Slip Wall	Representing the end of the domain, sufficiently away of the airfoil to interact with the features of the flow and it represents the way in which the air behaves when it is not affected by the airfoil.
Wall	Representing the surface of the Airfoil

Table 8: Boundary Conditions description.

It is mandatory to mention also that Turbulent Intensity of 0.02% and an Eddy viscosity ratio of 10 at the inlet and outlet order to achieve the same conditions than in the NASA experiments [2] and in Thomas Hansen study [1].

Moreover, the fluid used is air with a reference pressure of 1 [atm], it means that the pressure values obtained in the study will be relative to this absolute value as explained in equation 5; taking into account the density and dynamic viscosity from the Normal Conditions i.e. $\rho = 1.225\ \frac{kg}{m^3}$ and $\mu = 1.81 * 10^{-5}\ \frac{kg}{ms}$. Furthermore, the velocity set for the inlet is obtained from the equation 6:

$$P_{relative} = P_{absolute} - P_{reference} \tag{5}$$

$$V = \frac{Re\mu_\infty}{\rho_\infty L} \tag{6}$$

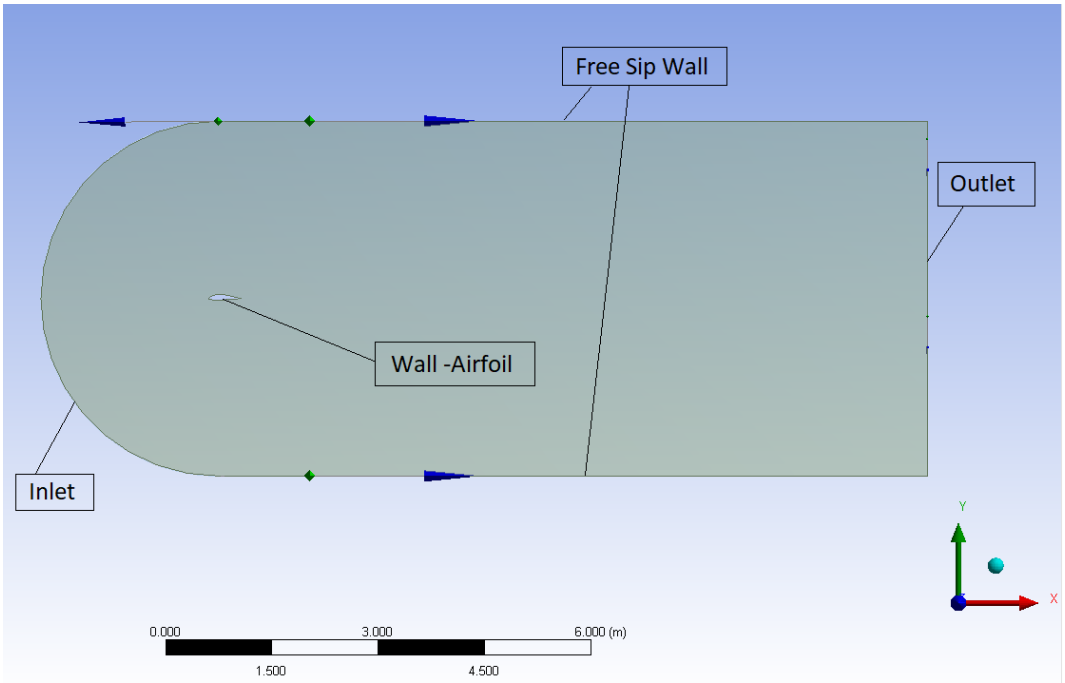

Figure 6: Boundary Condition distribution.

Which taking into account the Reynolds chosen for the study i.e. $1.5 \cdot 10^6$ and the characteristic length which is the chord (0.458 m) results as 47.86 m/s.

There were two turbulence models used in the solver set up, $k-\omega$ SST and Transition SST, both of them being set as a pressure based solver due to the non compressible features of the flow (if Mach number is below 0.3 the flow can be considered non compressible [6] shown in equation 7) using coupled solution for pressure an velocity in order to enhance the convergence and second order discretisation schemes were used in the non turbulent equations whereas first order schemes were used in the turbulent equations in order to achieve a more diffusive scheme improving the convergence of the solution [9]. The under relaxation factors were leave by default due to the good behavior in convergence of the simulations, so it was not consider necessary, for further studies, it would be interesting to increase them and see if it is possible.

$$M = \frac{V_\infty}{a} = \frac{V_\infty}{\sqrt{\gamma R T_\infty}} = \frac{47.87}{344} = 0.1392[-] \tag{7}$$

When talking about convergence criteria, the indications of Thomas Hansen Publication [1] were followed in order to simulate the conditions as similar as possible, so the residuals were kept to 10^{-4} . Moreover, other convergence criteria was added, the Lift and Drag coefficients should not change in the fifth decimal during 50 iterations before the convergence is achieved. The final convergence criteria adopted is the observation of the absence of spurious phenomenon in the control volume, which means that the flow should not have any kind strange behavior in the control volume simulated.

In the Oswald Factor calculation , the assumptions of the method used is to consider that the angles of attack studied are so close that the CD_0 is not a function of the angle of attack. Using the simulations of the glider for 0 [deg] of a.o.a. and the simulations of steady flight. By comparing the Drag Coefficients between the two angles of attack it is possible to obtain a system of equations in which the variables are the Oswald Factor and the CD_0 as shown in equations 8 and 9

$$e = \frac{CL_1^2 - CL_2^2}{(CD_1 - CD_2) * \pi * AR} \tag{8}$$

$$CD_0 = CD - \frac{CL^2}{\pi * e * AR} \tag{9}$$

3.1.4 Validation

The validation in this study is performed by comparing the main outcome of the study with the one performed by the NASA experimentally [2], and the main outcome of the 2D part is done regarding the aerodynamic parameters i.e. the CL and the CD which are obtained by equation 10:

$$CF' = \frac{Force}{q_\infty \cdot c} \tag{10}$$

Where the force must be replaced by Lift or Drag both in the main Force obtained from the simulation. Those forces are the main aerodynamic forces and it is interesting to remark that they come from the addition of two contributions, a part which is caused by he pressure field around the airfoil and another part caused by the friction between the fluid and the airfoil. For the actual purpose of this section the total value is computed by means of Fluent post processing tools. To finish with the description of equation 10, q_∞ is the dynamic pressure represented in 11:

$$q_\infty = \frac{1}{2} \cdot \rho_\infty \cdot V_\infty^2; \tag{11}$$

Where ρ_∞ is the density of the freestream and v_∞ is the speed of the freestream.

The validation is performed for 9.5 deg of angle of attack in order to use the same method for the rest of the cases and the validation data is shown in table 9. The validation was not performed with the angle of attack 10 [deg] because of the lack of data found in the NASA document.

Variables	DATA SST	DATA Transition	NASA
Lift Coefficient [-]	1.26	1.434	1.415
Drag Coefficient [-]	2.748E-02	1.649E-02	1.523E-02

Table 9: Validation data.

The relative errors are shown in table 10:

The Validation data show an strong correlation in the Transition SST model and a huge deviation in the SST model, which give a preliminary idea of the behavior

Variables	Diff SST [%]	Diff Transition [%]
Lift Coefficient	10.95	1.34
Drag Coefficient	93.52	8.27

Table 10: Validation errors.

the model will perform, in an industrial study, the SST model would be discarded but as the aim of this study is the comparison of both methods in order to find the best one for the project, it can be said that Transition model is validated with the reality and that preliminary SST model does have a great discordance with respect to the experimental data.

3.2 Results

The final outcomes of the study regarding the airfoil are depicted in this section. This section is composed of three different parts where the target information is explained and compared with the Thomas Hansen Study and thus with the data obtained by NASA experiments and XFOIL simulations.

First of all the main features obtained in the simulations were the Pressure Coefficients which is a measure of the change in static pressure in the airfoil surface, which is calculated by the formula expressed in equation 12 for two main cases following Thomas Hansen indications, which are 0 and 8.05 deg of angle of attack, in order to compare the solutions with the NASA experiments this correspond to figures 7:

$$CP = \frac{P - P_\infty}{q_\infty} = \frac{P - P_\infty}{\frac{1}{2}\rho V_\infty} \tag{12}$$

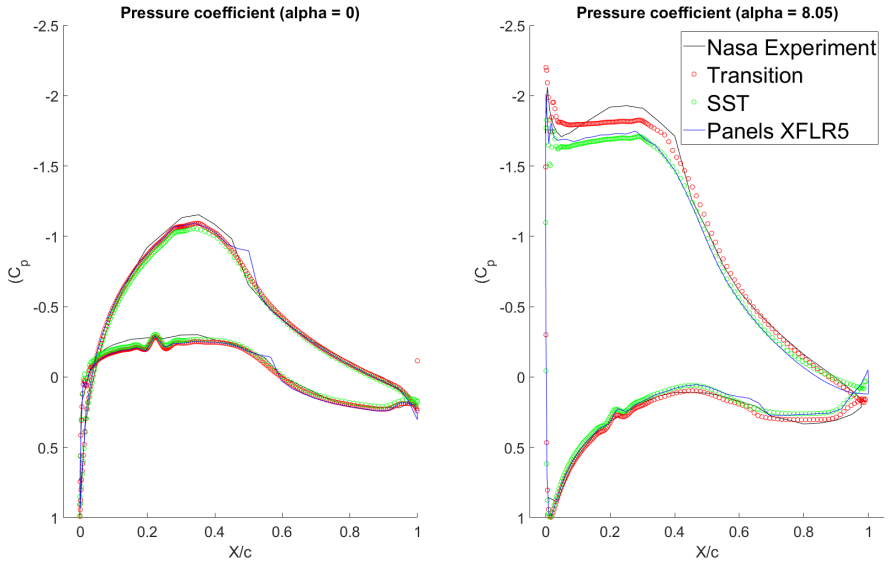

Figure 7: Comparison between $k-\omega$ SST, Transition SST, NASA data and XFOIL Pressure Coefficient for 0 [deg] (left) and 8.05 [deg] of a.o.a. .

It is possible to realize that the Transition SST model is slightly more similar to the NASA data than the $k-\omega$ SST which keeps more similarities with the Panel method implemented by XFOIL. It is also easy to see how there is an oscillation of the results given by Fluent and XFOIL in the upper part of the airfoil (represented in the lower line) which is not visible in the NASA data. The numerical data from the CP similarities is represented in 11

Another quite useful set of data is the one described by the Cl excursion with the angle of attack , which gives a good idea of the behavior of the airfoil in the most common range of performance. The comparison between the different sources of data, in this picture Thomas Hansen data [1] is also included in order to see the

Angle of Attack [deg]	Model	Average Error [%]	Max Error [%]
0	Transition	2.12	5.34
	SST	4.31	10.52
8.05	Transition	2.82	6.25
	SST	7.25	18.68

Table 11: Differences between Experimental and Simulation Data

similarities of the methods. The information obtained about the Lift coefficient vs the angle of attack is provided in fig 8 :

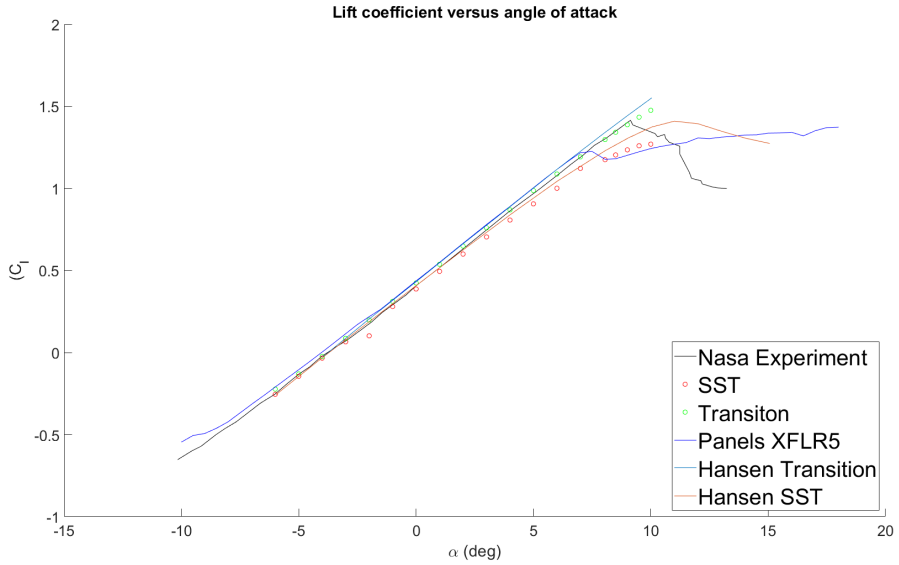

Figure 8: Lift coefficient vs angle of attack .

In figure 8, the great similarities between the different methods are clearly visible. However, it is important to clarify how the results of the Transition SST model are greatly similar to the experimental values of the NASA and how the $k-\omega$ SST has a point of failure when the stall arrives. Most of the models are essentially similar in the linear part of the graph but it is important to notify the bad performance of the CFD methods once the stall appears due to different reasons on each model which will be explained in section 3.3.

Another important parameter is the polar of the airfoil, the graph which expresses the behavior of the Lift Coefficient as a function of the Drag Coefficient, which gives a good representation of the trade off between Lift and Drag forces, which are translated afterwards into the Aerodynamic Efficiency, which is the ratio between the lift generated and the drag generated, depicted in equation 13 chart versus the angle of attack. Both of them are shown in figure 9a and 9b:

$$AE = \frac{L}{D} = \frac{q_\infty * c * CL}{q_\infty * c * CD} = \frac{CL}{CD} \tag{13}$$

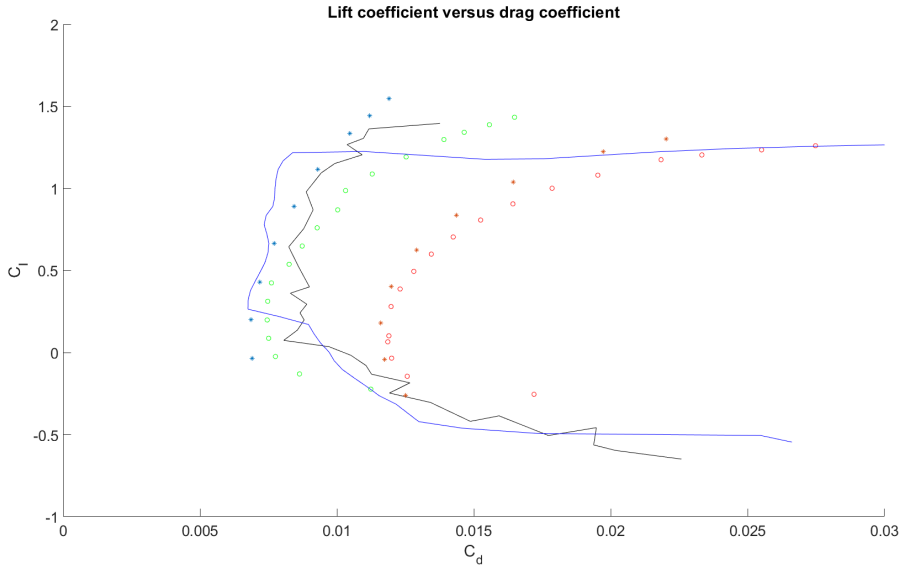

(a)

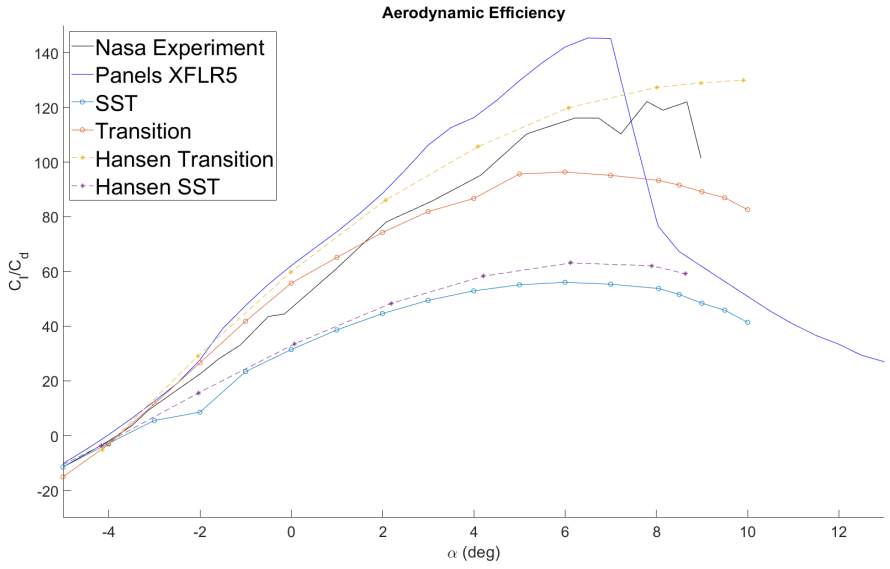

(b)

Figure 9: Airfoil polar (a) and for Aerodynamic Efficiency (b).

It is possible to see how the data obtained from simulations overestimates the Drag coefficient both in the Transition SST and in the $k-\omega$ SST. The models more similar to the NASA experimental behavior are the Transition SST both in Hansen data and in the simulations performed in fluent.

A more descriptive image will be given by the Turbulent Kinetic Energy, which is the kinetic energy produced by the instantaneous values of the velocity generated in Turbulent Flow represented in equation 14, which will show one of the most

important drag sources along the airfoil, which is depicted in figures 10 and 11. $k-\omega$ SST contours are the ones in the upper part and Transition SST contours are the ones in the lower part in each plot:

$$TKE = \frac{1}{2} * (\bar{u'^2} + \bar{v'^2} + \bar{w'^2}) \tag{14}$$

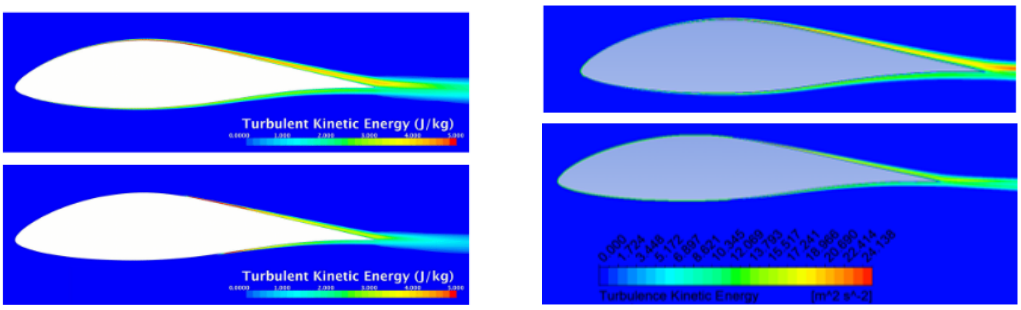

(a) (b)

Figure 10: TKE in Transition SST for Hansen studies REPRINTED WITH PERMISSION (a) and Fluent Studies (b) for 0 [deg] of aoa.

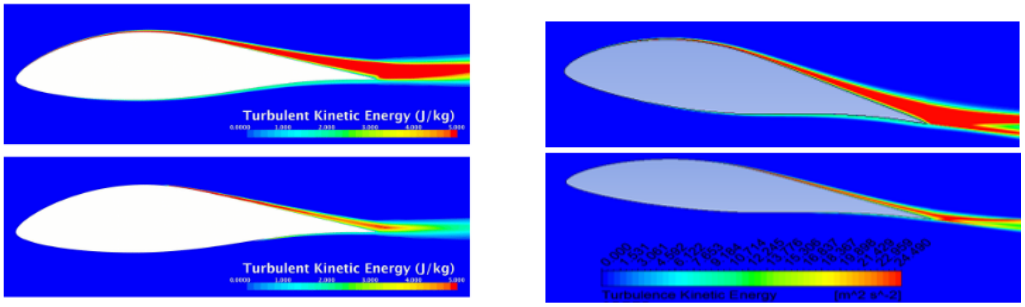

(a) (b)

Figure 11: TKE in $k-\epsilon$ SST for Hansen studies REPRINTED WITH PERMISSION (a) and Fluent Studies (b) for 8.05 [deg] of aoa.

Although the shape of the TKE increase is very similar, it is easy to see how the values of this study are greater than the Hansen studies as it happened with the Drag Coefficient, but not in the same scale, it is visible that the maximum TKE in Fluent simulations is overestimated by 5 times.

Given the results shown in figures 10 and 11, some additional simulations were performed in order to find a feasible reason for this miss match among the results. The simulations were performed with an adimensionalised chord, i.e. the chord was set to 1 [m] adapting the mesh setup with the only modification of the Boundary Layer treatment due to the change in length and therefore in freestream velocity by means of equation 4. The freestream velocity was obtained from equation 6 obtaining a value of 21.91 [m/s]. It is mandatory to mention that that due to the dynamic similarity the CL and CD values obtained had a 0.2% of error between the adimensional and realistic chord. The results for the Turbulent Kinetic Energy plots in the airfoil are shown in figures 12a and 12b:

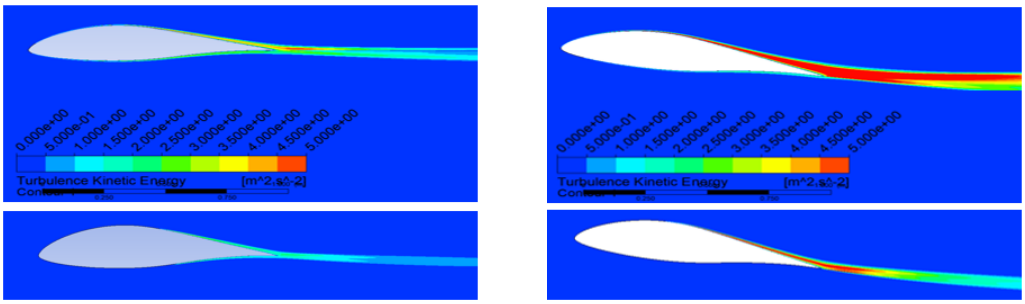

(a) (b)

Figure 12: TKE for a simulation with adimensional chord for 0 [deg] and 8.05 [deg] of a.o.a..

Now the comparison between Thomas Hansen results (shown in figures 10a and 11a) and the results of the simulation with adimensional chord in Fluent (figures 12a and 12b) are able to predict results which are strongly related, with the same scale, the representations of both cases show contours with the same TKE patterns. In section 3.3 this phenomena will be more deeply explained.

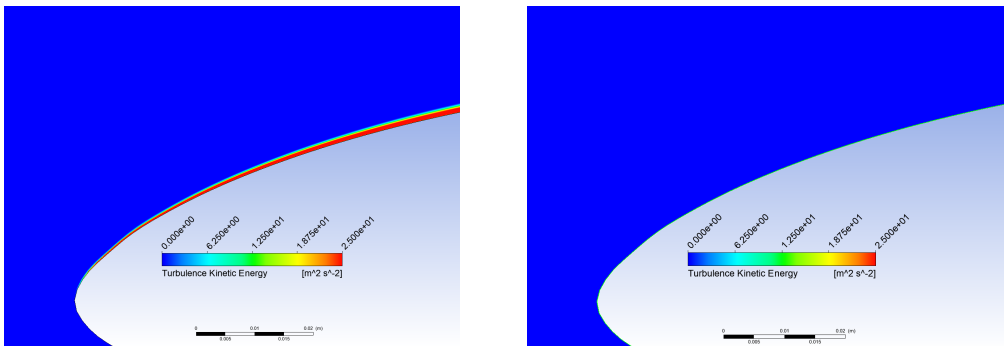

(a) (b)

Figure 13: Detail of the TKE in leading edge of the airfoil at 8.05 [deg] of a.o.a. for SST model (a) and Transition SST (b).

The detail shown in figure 13 of the TKE in the airfoil first part, and a nice outcome is shown in the detail, it is visible how the different turbulence models interact with the Boundary Layer. As shown in figure 13a, the SST model predicts generation of TKE from the begining and the transition model does not as depicted in figure 13b. In figure 14 the transition position in an adimensional chord is depicted with respect to several angles of attack. It is shown how the Extrados transition location is closer to the leading edge and how the opposite phenomenon occurs in the Intrados.

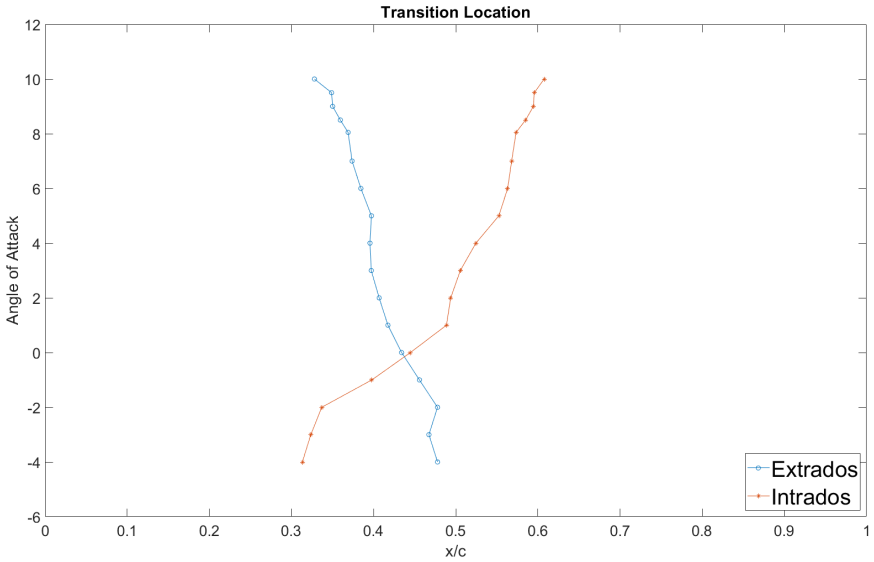

Figure 14: Transition position along the chord for different angles of attack

It is shown how the Extrados transition location is closer to the leading edge and how the opposite phenomenon occurs in the Intrados.

One could think that with the results shown it is enough to choose the Turbulent model which is going to be used in the 3D study, but the sources of the main aerodynamic parameters should be discused and more specificallly where the differences are bigger between both models. Therefore, the Drag Decomposition is shown in figure 15. Here is possible to see that the Drag Coefficient is a 150% bigger in the SST than in the Transition SST and it is remarkable how the Pressure Drag increases with the same trend in both models with respect to the Angle of Attack.

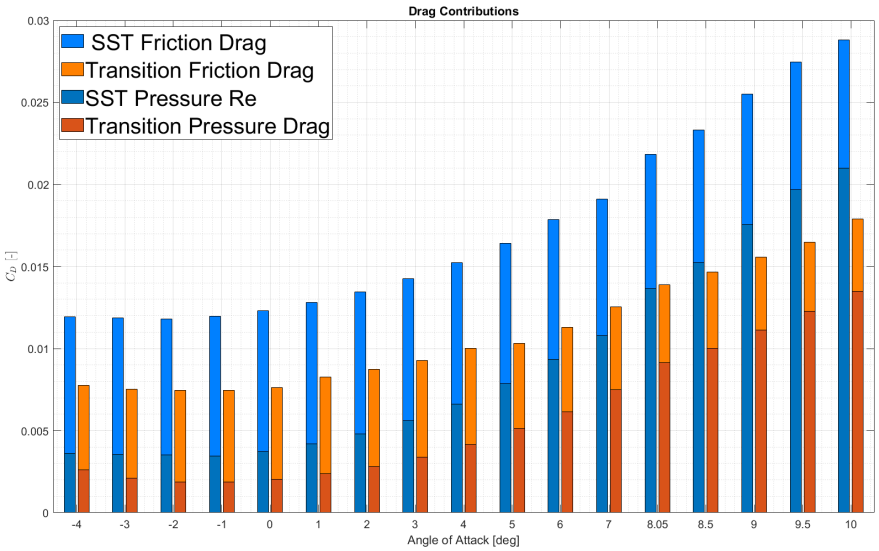

Figure 15: Drag Coefficient Decomposition between Pressure Drag and Friction Drag

Furthermore, the airfoil wake has an incredibly important implication in the Drag Coefficient, due to the high pressures that create in the wake and the detachment of the flow caused by the high pressure area. Thus, the wake has an incredibly big effect in the Drag coefficient estimation, and as it is shown in figure 16 the estimation of the vortex length in both models differ significantly. It is also remarkable that the ratio between the length and the height of the wake is mostly constant along the angles of attack and in both models the ratio is 3.

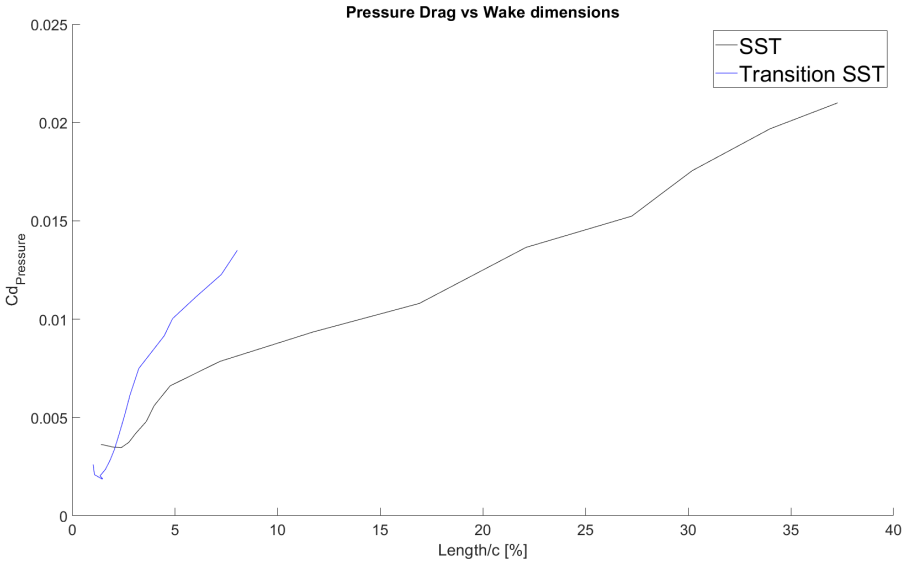

Figure 16: Cd pressure vs the Vortex dimensions

3.3 Discussions

Provided the results depicted in the previous section, a few comments must be done in order to explain the different features and outcomes of the study.

The Pressure coefficient depicted in figure 7, gives another idea of the performance of the CFD methods compared to the NASA experiments and the XFOIL simulations, and it seems obvious that they do it quite accurately, but in order to compare them more intensively, it must be commented than the Transition SST is the one which more similar look when comparing to the NASA data, even thought both models perform in a similar way, it is possible to realize that the similarities between the simulations and the experimental values are higher in the Transition model as shown in table 11. If the reader looks at equation 12, will understand that the outcome which can obtain with respect to the Pressure Coefficient is that the Static Pressure in the turbulent model is higher than in the transition one which following the Bernoulli equation in incompressible flow leads to explain that the speed in extrados in the zone between 10 and 40 % of the chord is higher in the transition model than in the SST model. Analysing this figure together with figure 2, it is possible to conclude that this zone previously mentioned is the one in which the transition phenomena occurs and this is obviously not taken into account in the fully turbulent model, but it is taken into account in the transitional one. Furthermore, the difference between the transition model and the experimental values can be explained by the model itself. As commented previously in the Theoretical background the Transition SST model uses semi-empirical correlations to predict the behavior of some of the most determinant variables which describe the flow, and even if the similarities with the experimental data are more than acceptable, it is mandatory to remind that being in the RANS spectrum, there are a lot of variables an assumptions that create these types of differences between the simulations and the reality. It can be seen that in the Pressure Coefficient figure, the separation bubble and the turbulent reattachment is obtained for the model Transition SST but with some error coming from the model.

When talking about the Lift versus angle of attack, it is necessary to explain the reason why the limits of the study were set in 10 [deg] of angle of attack and the reason is no other than it was checked that the results obtained in the simulations further than 10 [deg] were not consistent, i.e. the residuals would not arrive to the desired accuracy levels and they were very unstable, which is caused by the bad behavior of the RANS methods in these kind of problems where the flow is completely unstable as the zones related to the stall of an airfoil.
In figure 8 the lift coefficients of the study are shown together with the results obtained by Thomas Hansen [1], the XFOIL results and the NASA experiments. In this way, it is possible to reaffirm than the SST model behaves worse than the Transition in both Hansen and this study, performing better for negative and low angles of attack, but the error between the Transition and the NASA data is almost neglectable for the cases simulated in this study, the only difference worth to mention between the experimental results and the transition SST model is that it fails to predict the stall of the airfoil (given in the experimental data in 9 [deg]), because

instead of starting the Lift Coefficient drop after this value the trend of the line remains, which is another indicator of the behavior of RANS models with respect to the reality. When talking about the Lift Coefficient of the $k-\omega$ SST, it is possible to say that the differences with the experimental data are neglectable for the range of -4 to 5 [deg], where the prediction of lift coefficient starts to differ significantly from the transition model and the experimental data. For greater angles of attack it is possible to relate the bad behavior of the SST model with the apparition of the wake, which due to the nature of the model will grow significantly as it is shown in figure 16, this grow subtract effective surface where the lift is created due to the pressure difference. The pressure of the wake zone is as high as the freestream one due to the low speeds of the wake and thus, the amount of lift produced along the airfoil is slightly lower, but as the main part of the lift is created in the zones near the leading edge the difference is appreciable but not huge.

When it comes talk about the Drag Coefficient, figures 9a and 9b show the performance of the airfoil, showing respectively the trade off between Lift and Drag forces created and the Aerodynamic efficiency which is the ratio between Lift and Drag vs the angle of attack. Before doing any comment about the results it is mandatory that the Polar and the Aerodynamic Efficiency contain the same information, the only difference is that the Aerodynamic efficiency relates the ratio of CL and CD with the Angle of Attack in which they occur. In this picture is where it is possible to see how the panel method simulation starts to differ more from the NASA experiment provided that the pannel method comes from an inviscid model, which is modified to approximate the behavior to the reality, but not in the same level of accuracy than more complex models as CFD RANS models. It is also very interesting to see how Fluent simulations both SST and Transition, obtain greater values of Cd for the same Lift values than the ones performed in Star CCM+ by Hansen which is unexpected given the similarities of the simulations, in which the dynamic similarity was ensured. The overestimation of the drag coefficient with respect to the NASA experimental data is in the worst case scenario a 20 % for the transition SST model, which is not a neglectable error, but once more, taking into account the limitations of the RANS models which are more noticeable in the drag estimation due to the interconnection of this variable with turbulent features which make it even more difficult to analyze.

The most remarkable information given in figure 9b is that the greatest aerodynamic efficiency is obtained for the Transition SST in 6 [deg], 3 [deg] before the experimental data and Hansen results, but in the SST the biggest aerodynamic efficiency is obtained in 8 [deg] but with a lower value due to this overestimation of the Drag in both models, which is even more remarkable in the SST where the overestimation of the drag has a mean value of 60%. The final comment for this two images is that it is noticeable how the Transition SST completely outperforms the $k-\omega$ SST in the simulation of the reality, combining a much better estimation of the Drag Coefficient and a better estimation of the Lift Coefficient.

Looking at the TKE contours, the first impression in the comparisons provided in figures 10 and 11 seems that there is a huge overestimation of TKE in the sim-

ulations done in this study, but concerning the equation 14 [6], one can infer, that TKE is not related with the Dynamic Similarity obtained in this experiment, because depends on the average of the instantaneous speeds in the locations. In this study, the chord chosen has been the real measure of the root of the wing, but in Hansen's study, the chord was adimensionalized. Therefore, the speed is higher in this study than in Hansen's and this is the final explanation for this data. In order to make sure of this explanation two other simulations have been performed with an adimensionalized chord (shown in figure 12 and after that, the similarity with Hansen cases is completely fulfilled.

Once solved this problem, it is time to compare the solutions between the SST and Transition SST model. The TKE obtained in the fully turbulent simulation is quite big and it is caused by the own structure of the model which does not consider any laminar zones as it is shown in figure 13a where the production of TKE starts from the beginning and this creates a fully turbulent Boundary Layer from the beginning, and this fact joined with the rest of the parameters of the flow behavior along the airfoil creates a great area of high TKE in the rear part of the airfoil which continues in the zone occupied by the wake until it gets dissipated in the freestream flow once the perturbation created by the airfoil is far enough. On the other hand, it is visible that the TKE regions in the Transition model is significantly smaller and the values are also much smaller due to the later development of the turbulent region in the airfoil.
In order to see how the transition point develops in the Transition SST an additional process has been done obtaining the point of the airfoil in which the TKE starts to grow significantly. The transition from laminar to turbulent flow starts with this sudden increase of TKE, and this is how the extraction of the transition location has been done. As it is shown in figure 2 the turbulent region is bigger in the extrados when increasing the angle of attack but on the contrary it is smaller in the intrados. This fact is easily explainable if we consider the acceleration of the flow which occurs in an airfoil when increasing the angle of attack and following this reasoning one can deduce that the critical Reynolds will move forward (extrados because of the grater velocity) or backward (intrados because of the smaller velocity) [14] [15].

There is a great interest in the analysis of the decomposition of the Drag Coefficient in order to understand the mechanisms which create this force. As said before, the Drag Coefficient in 2D has only two components, which are the friction drag, which is caused by the Shear Stress in the x direction in the airfoil surface and the pressure drag, which is created by the forces of the pressure in the x direction, and it is mainly related by the wake as it is a feature of the flow which increases with the angle of attack and so is the Pressure Drag. When looking to figures 15 and 16 one can understand the differences in the drag estimation between in the transition model and the fully turbulent model, given that the friction drag is pretty similar for the two of them, the biggest difference between both models is the impossibility for the wake estimation of the SST, which creates a big overestimation of the drag.

3.4 Conclusions

After the completion of this 2D study some major conclusions have been obtained:

- After the completion of this study and the positive results obtained, it can be said that the methodology has been established.

- The main reason of the gap between the experimental results and the fully turbulent model can be divided in three parts. At low angles of attack the lift estimation is correct but it fails to predict the friction drag, which happens due to the fully turbulent treatment of the Boundary Layer increasing the friction. For greater angles of attack the lift coefficient is underestimated due to an over prediction of the wake dimensions which reduces the effective airfoil surface. This fact is also a consequence for the overestimation of the Pressure drag for those angles of attack. This behavior is produced by the fully turbulent nature of the model.

- Given the better performance of the Transition SST model, this will be the model used in advance for the 3D study of the whole body.

4 3D study: Glider Analysis

As commented in the Introduction, this study will focus in the performance of the glider in the vicinity of the best possible glide ratio, which corresponds to the range of speeds between 90 and 100 [kmh]. In this study the performance of the aircraft will be analyzed using the Transition SST turbulence model.

4.1 Method

4.1.1 Geometry

As done in the 2D study, the aim of the geometrical procedures is to obtain a control volume able to represent the fluid in the simulation. In this case, being a 3D body, instead of creating a surface for the subtraction, it is necessary to create a 3D body and then subtract the body of interest from the geometry created to obtain the control volume in order to achieve the fluid volume that will be studied. As commented in the introduction, in this section of the project the glider is going to be studied and, in order to achieve quality studies, it is necessary to divide the glider in two different parts, the fuselage with the wings and the fuselage with the empennage as shown in figure 17 .As it is shown in the figures, the initial geometry has already taken advantage of the Symmetry condition in the glider in order to improve the computational cost vs results ratio.
The process of the construction of the control volume was done in Design Modeler of ANSYS, and due to the nature of the geometry provided for this study by Thomas Hansen [1], which consisted on shells, some pre-process of the geometry was required. With the aim of converting the combination of shells into a usable volume, the small holes of the surface needed to be repaired and also another extra surface was needed in the symmetry plane of the aircraft. After this procedure, the ensemble of surfaces were joined as as a volume body. Afterwards, the only required operation was the subtraction of the body from the bigger volume which was created following Thomas Hansen's indications. A quart of sphere of 50 [m] of radius and half a cylinder with 50 [m] of radius and 100 [m] of length were created to produce a big enough control volume for the development of the project. Once obtained the control volume, the next step was the creation of the "frozen" geometry due to the need of refining the mesh in the zones close to the aircraft. This frozen geometry, also known as Body of Influence (BoI) has two parts, one created in the vicinity of the fuselage (for both Main Body and Empennage), which has a geometry of a half a cylinder with 3 [m] of radius and 20 [m] of length and one dedicated body for the wing or the horizontal stabilizer depending on the body of application, which ensures of the refining of those the body.

(a)

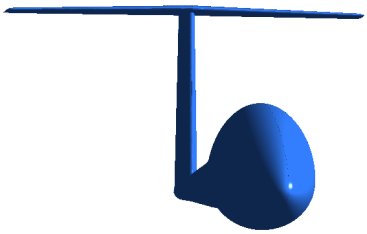

(b)

Figure 17: Geometry of the main Body (a) and the empennage body (b).

In this study, the improvement chosen for the Standard Cirrus Glider was the addition of a Winglet in the wing. This Winglet was created in Catia V5 and was performed in 3 different operations. The first step consisted on cutting the existing wingtip, due to the features that the aircraft already has in this zone 10 cm of wing had to be removed in order to make the modifications possible. Afterwards, the next operation was the extrusion and extension of the airfoil 0.3 [m], and the last step involved the rotation of these new surfaces which form the winglet. It is to be said that according to the literature [16], gliders winglets are usually 90 [deg] with respect to the wing, and that is what has been done in this project. The geometry of the glider with the winglet used is shown in figure 18. The winglet has also a sweep angle of 30 [deg]. The winglet geometry was built following the criteria of other gliders which already have this feature but with maintaining the airfoil of the wing to simplify the CAD work. It is mandatory to mention that the strategy followed for the construction of the Body of influence is the same as the one used in the original geometry. The improved geometry is shown in figure 18:

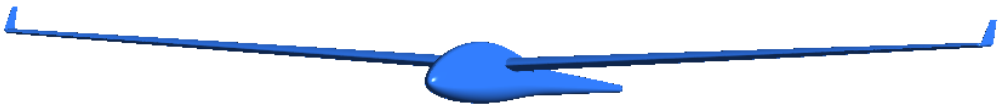

(a)

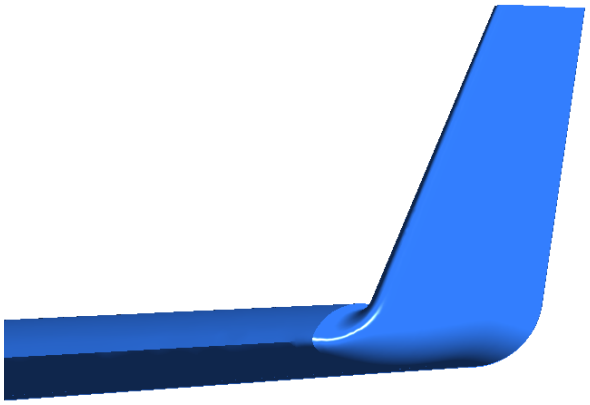

(b)

Figure 18: Winglet main body (a) and detail of the winglet (b).

4.1.2 Mesh

In contrast with the mesh used in the 2D study, the mesh used in the 3D study is non structured and the elements used for the mesh have been a combination between tetrahedrons and prisms. The first ones were used in the external mesh and in the Body of Influence while the prisms were used for the Boundary layer treatment. The structure of the mesh consisted on a surface mesh in the glider surfaces in order to ensure to capture the important features of the body. This mesh is the core of the study and several refinements an methods were used until the best possible surface mesh was obtained, trying to make sure that the real geometry of the glider was actually captured by the mesh. After the surface mesh was obtained, the Boundary Layer treatment was set up. Due to the features of the turbulence model used , Transition SST, it is needed to ensure a Y+ of 1 in the glider surface and in order to do so, the Y+ calculator of Pointwise [17] which uses the Flat Plate approach to calculate the First Height of the Boundary Layer Thickness in order to get the desired Y+ for a given experiment. In order to be sure about the Y+ behavior around the aircraft, the meshes were built in order to achieve Y+ = 1 for a higher velocity than the one desired, this is, to obtain a Y+ for 160 [kmh]. The first layer of the Inflation created for the Boundary Layer was $6.9 * 10^{-6}$ [m] and 40 layers using a growth rate of 1.1 following Thomas Hansen indications[1]. The last part of the mesh settings was the set up of the Body of Influence around the glider, which resulted, after the mesh independence study, in a specific length of element of 0.1 [m]. An example of the mesh configuration for the Front part of the aircraft is shown in figure 19

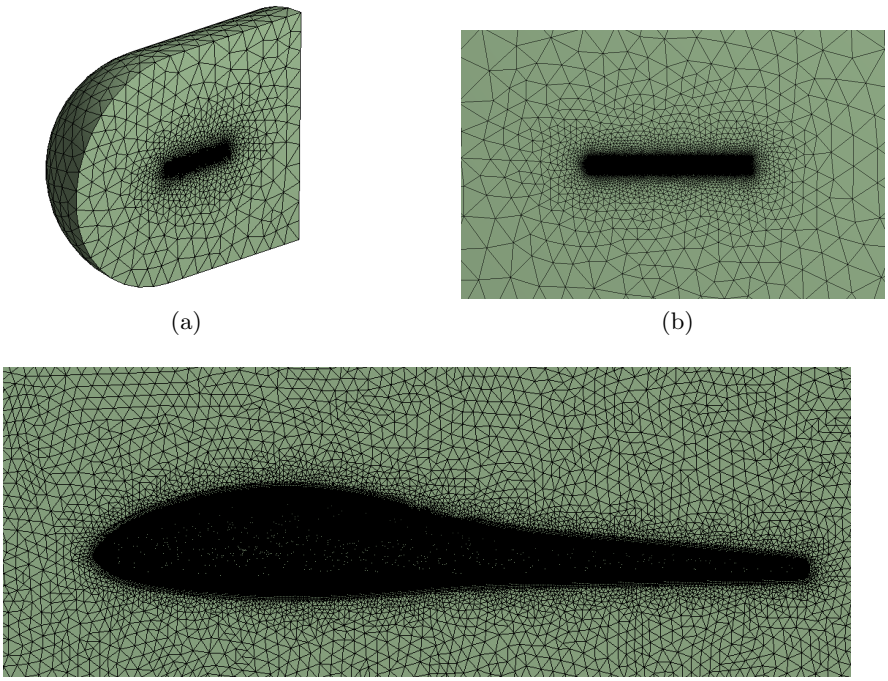

(a) (b)

(c)

Figure 19: Mesh example of the geometry. Whole Domain a), Body of Influence b) and example of the glider geometry c)

As in the previous paragraph, a mesh independence study was performed to ensure of the correct behavior of the mesh, and it was performed for both, Main Body and Empennage. This study was performed for both bodies in a configuration of 0 [deg] of angle of attack and with an airspeed of 160 kmh. This election was done with the aim of proving that the mesh was completely useful for every condition simulated in during the study, being this speed never overtaken. The data concerning the Mesh independence studies of both bodies is shown in tables 12 and 13:

Variables	**Coarse**	**Medium**	**Diff**	**Fine**	**Diff**
Elements	6 M	14 M	-	32 M	-
Lift Coefficient	0.626	0.615	1.721%	0.603	1.99%
Drag Coefficient	$1.768 * 10^{-2}$	$1.638 * 10^{-2}$	7.353%	$1.654 * 10^{-2}$	0.977%
Max speed [m/s]	66.97	67.013	0.06%	67.015	0.00%
Pressure Probe 1 [Pa]	301.80	336.32	11.44%	316.34	5.94%
Pressure Probe 2 [Pa]	-809.98	-787.02	2.84%	-798.02	1.40%
Pressure Probe 3 [Pa]	101.57	91.29	10.12%	89.00	2.51%
Pressure Probe 4 [Pa]	-61.89	-35.11	43.27%	32.29	8.03%
Pressure Probe 5 [Pa]	-1001.27	-969.99	3.12%	-993.88	2.463%
Pressure Probe 6 [Pa]	84.00	69.00	17.86%	69.03	0.04%
Integrated Shear Stress [N]	40.92	31.29	22.22%	31.00	2.87%
Mean error			12.00%		2.89%

Table 12: Mesh independence study for the Main Body.

Variables	**Coarse**	**Medium**	**Diff**	**Fine**	**Diff**
Elements	7 M	11 M	-	21 M	-
Lift Coefficient	$2.56 * 10^{-2}$	$2.56 * 10^{-2}$	0.00%	$2.56 * 10^{-2}$	0.00%
Drag Coefficient	$3.34 * 10^{-3}$	$3.34 * 10^{-3}$	7.353%	$3.34 * 10^{-3}$	0.98%
Max speed [m/s]	60.97	60.97	0.00%	60.97	0.00%
Pressure Probe 1 [Pa]	91.43	87.68	4.10%	87.86	0.20%
Pressure Probe 2 [Pa]	-39.05	-45.73	17.09%	-46.39	1.42%
Pressure Probe 3 [Pa]	19.81	14.30	27.80%	13.91	2.75%
. **Pressure Probe 4 [Pa]**	28.35	23.74	16.29%	23.61	0.51%
Pressure Probe 5 [Pa]	-159.72	-165.68	3.73%	-165.949	0.16%
Pressure Probe 6 [Pa]	112.958	106.83	5.42%	107.09	0.04%
Integrated Shear Stress [N]	4.62	4.61	0.30%	4.61	0.00%
Mean error			8.30%		0.59%

Table 13: Mesh independence study for the Empennage.

According to the information shown in tables 12 and 13, the meshes chosen for the study are the medium ones due to the fact that they provide the best ratio between the computational cost and the accuracy of the results. The location of the Pressure proves for the different geometries are shown in Appendix A.

4.1.3 Solver

The Boundary Conditions are the same in all the different geometries, the only difference is found in the amount of surfaces of the glider depending on the case analyzed. The general Boundary Conditions used in the study are shown in table 14 and represented in figure 20.

Inlet	A constant velocity inlet directed by a vector in the X direction and given by the particular case analyzed (from 25 to 27.78 [m/s])
Outlet	An static pressure outlet with the absolute pressure set to 1 atm in order to represent the absence of perturbation in the outlet
Free Slip Wall	Representing the end of the domain, sufficiently away of the glider to interact with the features of the flow and it represents the way in which the air behaves when it is not affected by the airfoil.
Wall	Representing the surface of the Glider for the three different geometries.
Symmetry	Representing the symmetry plane of the glider and reducing the computational cost by two.

Table 14: Boundary Conditions description.

In order to keep the study smilar to he reality, some advanced features were set in the inlet and outlet in the same way that in the 2D study. The Turbulent Intensity was set to 0.1% and the Eddy Viscosity Ratio to 10, to maintain the similarities with Thomas Hansen study [1] and to implement the most realistic conditions in order to compare the results with the experimental study of IDAFILEG [3].

As it is usual in this type of simulations, the air is used as the fluid and the normal conditions are implemented. Due to the speeds used in this simulation the air is considered as an incompressible fluid (by means of equation 7 it is checked that the Mach number is in the range [0-0.3] for each simulation). The reference pressure is set to 1 atm, and density and dynamic viscosity are considered as in Normal Conditions of air at 25 $[deg]C$ i.e. $\rho = 1.225\ \frac{Kg}{m^3}$ and $\mu = 1.81\ \frac{Kg}{ms}$.

One of the conclusions of the 2D study was the election of the turbulence model and as commented in Section 3.4, the turbulent model Transition SST has been used in this simulations due to the better adaption to the reality. The standard settings for a turbulent incompressible simulation are chosen for the discretisation scheme. This stands for coupled velocity and pressure, second order schemes for the non turbulent variables and first order schemes for the turbulent variables .

When it comes to talk about the convergence conditions, the residuals were set to 10^{-5}. Furthermore, two more convergence conditions were added to make sure that the Lift and Drag Coefficient did not vary in the fifth decimal for at least 50 iterations following Thomas Hansen's indications.

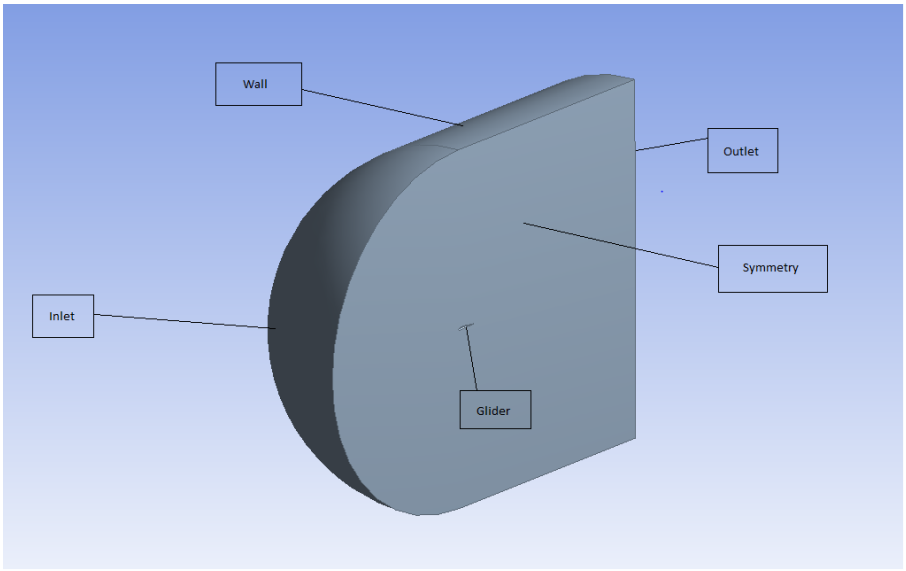

(a)

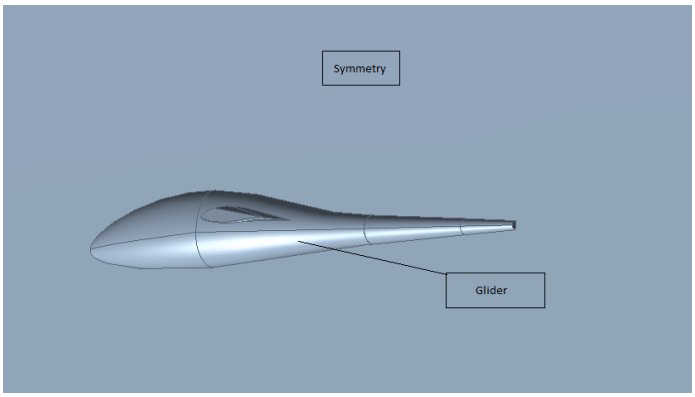

(b)

Figure 20: Boundary Conditions location (a) and detail of the glider surface in the control volume (b).

4.1.4 Method for the extraction of the results

The first thing one must take into account is the bodies in which the glider is divided. As commented in section 4.1.1 the glider is divided in two different bodies, one formed by the wings and the frontal part of the fuselage (see figure 17a) and the rest with the whole fuselage and the empennage (see figure 17b). Despite the division of the geometry is beneficial for the simulations convergence, it makes slightly challenging the way in computing the forces. In order to avoid computing the same surface twice, it is mandatory to define the surfaces during the meshing process or in the post process by means of Iso Clips . In this project the second methodology has been applied. An Iso Clip was created on each geometry dividing the geometries in two parts as shown in figure 21:

(a) (b)

Figure 21: Zones of result gathering : main body a) and empennage b)

The use of this method, allows to calculate the variables of the aircraft in an easy way and with a great accuracy. In the winglet geometry the same method has been used but the winglet has been separated from the wing in order to be able to obtain its contributions to the aircraft performance.

The aim of this study is to get the steady flight conditions, in order to perform compare it with the experimental performance values. The procedure relies in the low angles of attack in which the steady flight is developed which coincides with the linear behavior of the lift coefficient [18]. The main difference between the Cl-α of a 2D case and a 3D case is the slope of the linear zone. In a 2D case, the equation of the linear zone of the Cl slope is represented in equation 15 and the slope is π, whereas the 3D slope depends on some geometrical parameters represented in equation 16 [19]:

$$Cl_{2D} = Offset + \pi * Angleofattack(rad) \tag{15}$$

$$Cl_{3D} = Offset + \frac{Cl_{2D}}{1 + \frac{Cl_{2D}}{AR*\pi}} \tag{16}$$

Where AR is the aspect ratio which stands for the formula shown in equation 17 where b is the span of the wing:

$$AR = \frac{b^2}{WingArea} \tag{17}$$

Following this reasoning, it is accessory to obtain two different points of the line in the linear zone for each speed in order to be able to predict the configuration of the aircraft which provides the lift coefficient needed for the steady flight. The angles of attack chosen for the preliminary study where 0 [deg] and -3.5 [deg] and the results of this study are shown in table 15:

Study Outcomes				
Speed [kmh]	AoA [deg]	Cl Body	Cl Emp	CL
90	-3.5	0.258	3.00E-04	0.259
	0	0.624	2.60E-02	0.650
95	-3.5	0.289	4.20E-04	0.289
	0	0.632	2.61E-02	0.659
100	-3.5	0.321	4.00E-04	0.322
	0	0.633	2.61E-02	0.659

Table 15: Results of the preliminary simulations.

With this information the equation of the Lift Coefficient vs the angle of attack can be obtained solving for y_0 and m equation 18. By means of the Steady Flight Condition and the Lift equation (19), the required Cl is obtained.

$$Cl = y_0 + m * AoA \tag{18}$$

$$Weight = Lift = \frac{1}{2} * \rho_\infty * V_\infty * WingArea * CL \tag{19}$$

The coefficients together with the angle of attack necessary for the steady flight Lift Coefficient are shown in table 16:

Speed [kmh]	y_0	m	Cl	Aoa [deg]
90	0.650	0.112	0.910	2.327
95	0.659	0.105	0.817	1.501
100	0.659	0.096	0.737	0.805

Table 16: Solutions for equation 18 and Angle of Attack obtained for the steady flight

4.1.5 Validation

The validation of the model gives information the simulation results compared with the experimental values. The experimental data provided by IDAFLIEG study [3] is relative to the steady flight condition. In order to be able to validate the method, some simulations which are shown in Results 4.2.1 have been developed in order to achieve the data for the validation. The aerodynamic efficiency has been chosen to validate the data shown in table 17:

Speeds	**DATA IDAFLIEG**	**Simulation**	**Error [%]**
90 [kmh]	35.98	33.58	6.68
95 [kmh]	36.38	34.79	4.35
100 [kmh]	36.32	34.98	3.68

Table 17: Validation data.

Even if an error of 5% is obtained, due to the complexity of the study and the

aim of the study itself, the validation is accomplished.

4.2 Results

The results of the 3D study are depicted in this section, where the performance of the steady flight conditions are going to be evaluated together with the experimental results and also the calculation of the Oswald Factor for the wings are going to be obtained. Finally, the evaluation of the addition of a winglet is going to be studied.

4.2.1 Glider Performance

Once the glider's steady angles of attack are obtained, it is possible to compare the behavior of the glider with respect to the experimental measurements of IDAFLIEG [3].

The parameter most closely related with the steady flight is the Lift coefficient, due to the fact that depending on the flight speed, the angle of attack needed for obtain the sufficient amount of Lift force to compensate the weight of the Aircraft. These angles have been already calculated in the previous section and the comparison of the results of the Lift Coefficient vs the angle of attack is shown in figure 22;

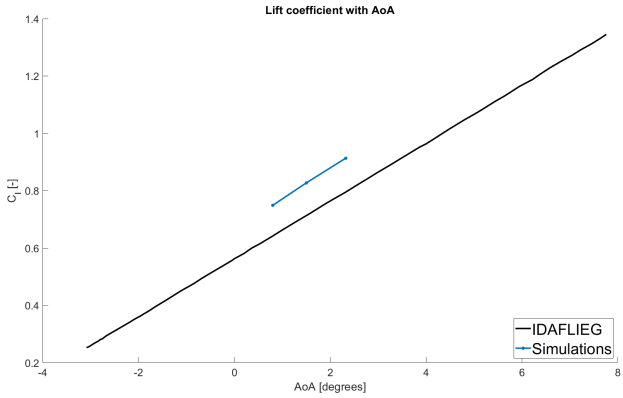

Figure 22: Lift coefficient vs angle of attack .

It is possible to see how both lines have the same slope which gives an idea of the similarities in the behavior between the simulation and the experimental data , but it is mandatory to comment the offset of 1 [deg] approximately between the measures which relates an overestimation of the Lift created in the model with respect to the experimental data. This does not mean that the simulations performed do not fit the steady flight condition, but means that the angle of attack used to achieve this condition is slightly lower. It is also possible that the application of the symmetry simplification may have some influence in the results of the performance analysis, although it must be a minor error. Finally, there may be some differences in the geometry simulated and in the one used in the experiments, which may take

part in the offset.

The next important value which is necessary to analyze is the Drag coefficient, which is the value which will determine the time the glider will be able to stay airborne. In figure 23 is possible to observe an small overestimation of the Drag Coefficient with respect to the experimental values. The trend of the curves are significantly similar. The average error of the CD with respect to the Experimental conditions is 6.23%.

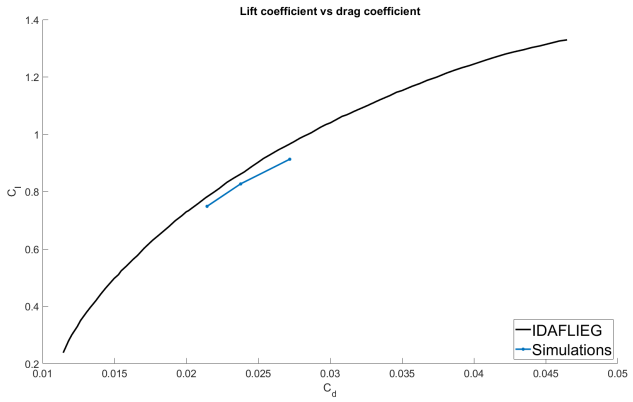

Figure 23: Relation between Cl and Cd.

The next images of the performance of the aircraft are mainly a relation between the former variables. The first parameter will tell which is the aerodynamic efficiency of the steady flight, which means that instead showing the aerodynamic efficiency with respect to the angle of attack of the aircraft it will show the variable with respect to the flight speed. The Aerodynamic efficiency is shown in figure 24. Due to the scale the difference between the values seem large, but after computing the error, the value obtained as an average is around 5%. The maximum Aerodynamic efficiency is located in 100 [kmh] and it is 34.96.

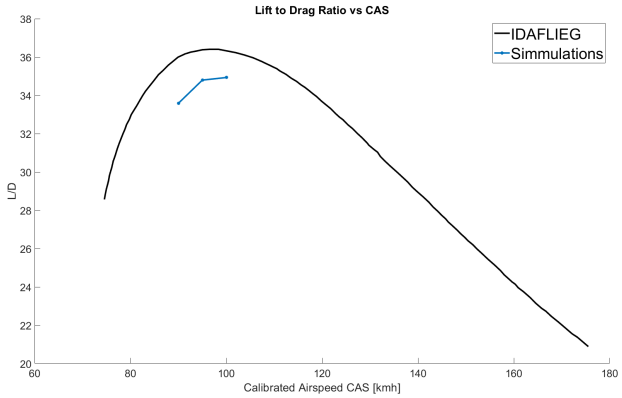

Figure 24: Aerodynamic efficiency for the steady flight.

The last graph concerning the performance of the aircraft is the sink ratio graph which actually is one of the most important ones. It represents the vertical velocity

that the aircraft inherently has while gliding at the steady speed. The formula of the sink ratio is shown in equation 20 [20]:

$$SinkRatio = h = V * \sin(\phi) \tag{20}$$

Where h is the vertical speed which is present in the glide path in [m/s], V is the flight speed in [m/s] and ϕ is the glide angle represented in equation 21:

$$\tan\phi = \frac{1}{AE} \tag{21}$$

The sink ratio for the steady flight is shown in figure 25 where it is possible to see how similar the simulations perform with respect to the experimental measurements:

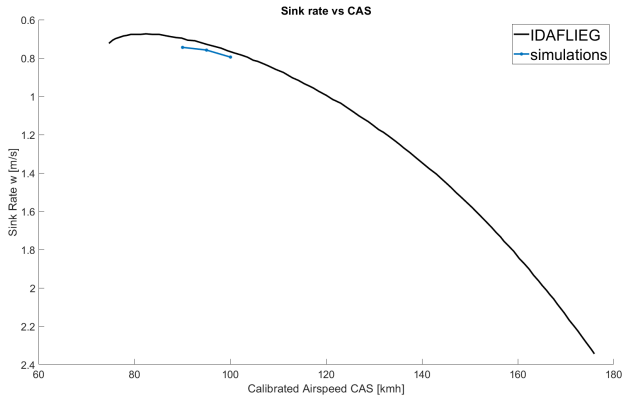

Figure 25: Sink Rate for the steady flight.

To end this section, the glide ratio, which is represented in equation 22, is analyzed:

$$GlideRatio = \frac{V * \sin\phi}{h} \tag{22}$$

Where h is the sink ratio and V is the aircraft speed both in [m/s].

The maximum glide ratio in the experimental measurements is found flying at 94.47 [kmh] being this one 36.51, whereas in the speeds analyzed in the simulations the maximum value is found in 100 [kmh]. Th information about the glide ratio calculated in the velocities simulated are shown in table 18:

Speed [kmh]	Glide Ratio [-]
90	33.60
95	34.81
100	34.94

Table 18: Glide ratios for the analyzed speeds

4.2.2 Oswald factor

In the 3D spectrum, the Drag Coefficient is not only formed by the Pressure and Friction Drag, but also the one from the Wing Tip vortex created by pressure difference between the upper and lower surfaces of the wing. This happens because the lift generation creates a pressure difference between the upper (low pressure) and lower (high pressure) surfaces (see figure 26) which meet at the wing tip and as a result of this pressure difference, the air from the lower surface tries to go towards the upper surface creating in that way the wing tip Vortex, the responsible of the Induced Drag. Figure 27 and 28show different representations of this wing tip vortex.

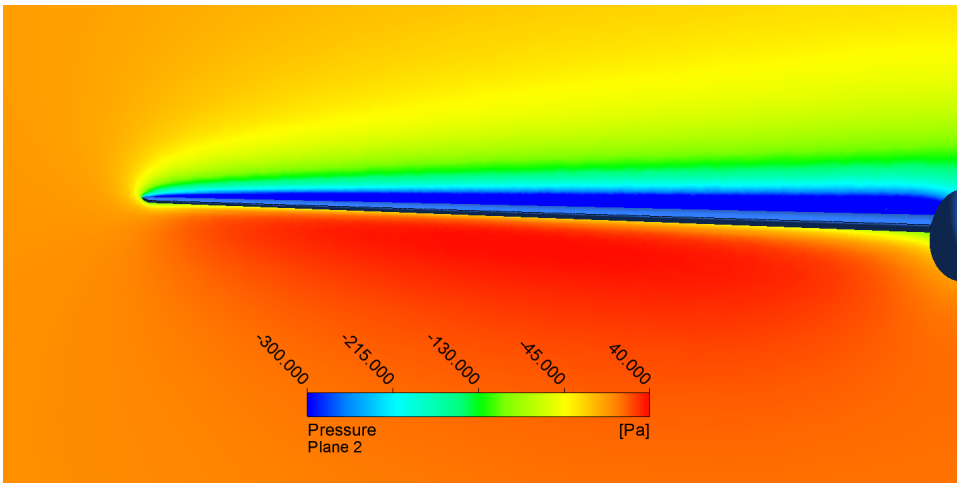

Figure 26: Pressure difference between the upper and lower surfaces.

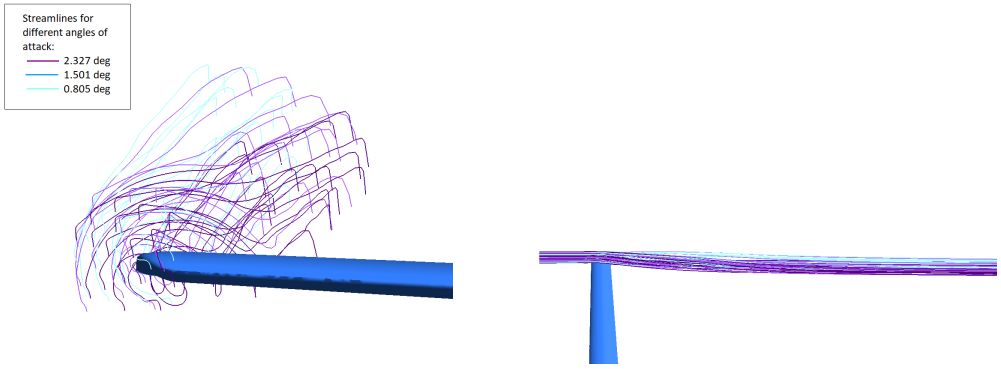

(a) (b)

Figure 27: Curvature of the streamlines due to wing Tip Vortex for the steady flight front View a) and Top View b)

In figure 27 the effects of the wing tip vortex in the streamlines around the wing tip is shown. As it is appreciable in the image, the higher the angle of attack, the bigger the distortion and the curvature added to the streamlines.

Figure 28 show a pressure contour in the wing tip for the case of 2.327 [deg] which represents the y and z components of the velocity in the surroundings of the

Wing Tip, which gives an idea of the effect that the Wing Tip Vortex creates in the flow and explain the cause of the streamline curvature of figure 27.

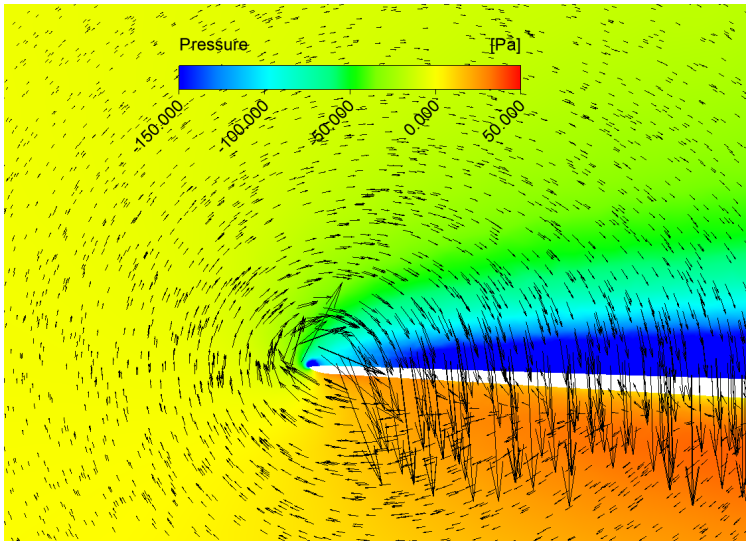

Figure 28: Contour of the pressure in the wingtip and representation of the Z and Y components of the Velocity.

When it comes to talk about the wing tip vortex it is mandatory to explain the effect that it has in the Drag coefficient. As commented in the Theoretical Background, in 3D the Drag Coefficient can be decomposed as shown in equation 23 considering the flow subsonic (below the critical Mach number):

$$CD = CD_0 + CD_i = CD_0 + \frac{CL^2}{\pi * e * AR} \tag{23}$$

Where CD_0 is the drag created by the aircraft in 0 Lift conditions and CD_i is the induced drag or lift induced drag which depends on the Lift Coefficient, AR which is the aspect ratio (see equation 17) and e is the Oswald factor, a form factor which compares the aircraft wing with an elliptical wing, which is the Wing geometry which reduces most the Induced Drag.

Usually the calculation of Oswald Factor is a complex procedure. Given the fact that Oswald Factor is a geometrical factor which takes into account different measurements of the wing which are not always available and are very costly to perform.

It is known that in steady flight the CD_0 and CD_i are function of the speed, but in the case of the CD_i this happens because the angle of attack is a direct consequence of the speed for the steady flight. It can be said that the CD_0 is a function of the speed, but actually it also depends on the angle of attack, given the fact that the CD_0 is formed by the friction drag (function of the speed) and the (pressure drag) which depends also in the angle of attack.

The results of equations 8 and 9 are shown in table 19:

Speed [kmh]	AoA [deg]	Cl [-]	Cd [-]	Oswald [-]	Cd_0	Cdi
90	0	0.650	1.925E-02	0.733	1.110E-02	8.154E-03
	2.327	0.913	2.720E-02			1.610E-02
95	0	0.658	1.931E-02	0.795	1.160E-02	7.714E-03
	1.501	0.827	2.377E-02			1.2117E-02
100	0	0.659	1.924E-02	0.808	1.162E-02	7.614E-02
	0.805	0.749	2.145E-02			9.852E-03

Table 19: Solutions for equations 8 and 9

The average of the Oswald factor is 0.78. It is visible how the CD_0 increases with the speed and also how the CD_i is greater when the angle of attack is greater.

4.2.3 Winglet Results

The reason of application of the Winglets is the reduction of the Wing Tip Vortex, which reduces the induced Drag which has been proved as an effective measurement in the Drag Reduction. The less known advantage of Winglets is that it decreases the effect of the Downwash effect in the wing due to the reduction of transverse flow in from the lower to the upper surface, which increases the effective angle of attack of the wing .

In this section the angles of attack used by the glider are analyzed with the addition of a Winglet. As the only modification done has been performed in the front part of the glider, which is the front body geometry. The analysis is performed in this part of the geometry because no modification has been done in the empennage body, and it would only make the changes less visibles.

The values obtained from the simulations for the steady flight with the winglets are shown in table 20:

Vel [kmh]	95	100
Angle of Attack [deg]	1.501	0.805
CD Friction Body	6.159E-03	6.378E-03
CD Pressure Body	1.365E-02	1.128E-02
CD Friction Winglet	8.250E-05	8.499E-05
CD Pressure Winglet	4.248E-04	5.350E-04
CD Pressure Total	1.407E-02	1.182E-02
CD Friction Total	6.242E-03	6.463E-03
CD Total	2.031E-02	1.828E-02
CL	0.787818	0.714945

Table 20: Results of the Winglet simulations

The comparison between the drag of simulations with winglet and without winglet is depicted in table 21 where it is possible to see an small decrease in the drag coefficient which comes mainly from the decrease in Pressure drag. In the 95 [kmh] case, the Friction Drag difference is an spurious which does not follow the trend followed by the other velocity decreasing the friction drag in in the winglet case.

A comparison between the pressure perturbation of the flow after the wingtip is depicted in figure 29 where it is possible to see how the disturbance in the Winglet is smaller than the one in the original wingtip. The contours are located at 0.1 m, 0.3 m and 0.5 m of the wing end.

It is also worth mentioning the difference between the lift coefficient between the cases with or without winglet which are shown in table 22 which show an average decrease of 0.44 % in the lift coefficient generated.

Variable	Speed [kmh]	Winglet	No Winglet	Diff [%]
CD	95	2.031E-02	2.070E-02	-1.875
	100	1.828E-02	1.850E-02	-1.196
CD Pressure	95	1.407E-02	1.422E-02	-1.053
	100	1.182E-02	1.210E-02	-2.350
CD Friction	95	6.242E-03	6.503E-03	-4.019
	100	6.463E-03	6.390E-03	1.143

Table 21: The comparisons between the drag components in the different cases studied

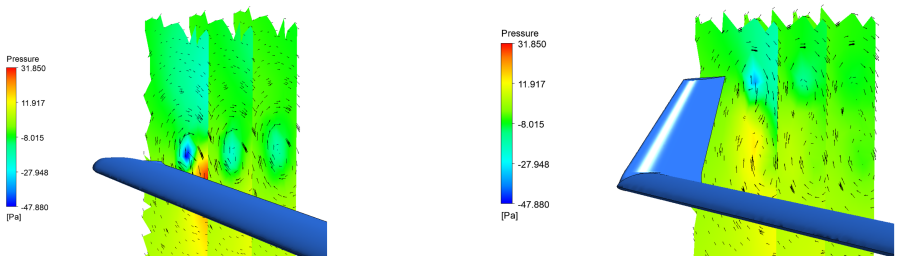

(a) (b)

Figure 29: Curvature of the streamlines due to wing Tip Vortex for the steady flight front View a) and Top View b)

Speed [kmh]	Winglet	No winglet	Diff [%]
95	0.788	0.792	-0.465
100	0.715	0.718	-0.425

Table 22: Lift coefficient comparison between the cases studied

Another interesting feature is the lift distribution along the wing, because it has an important repercussion with respect to the aircraft efficiency, the more similar to the elliptic wing distribution, the more effective the wing is The different cases studied are shown in figures 30 and 31:

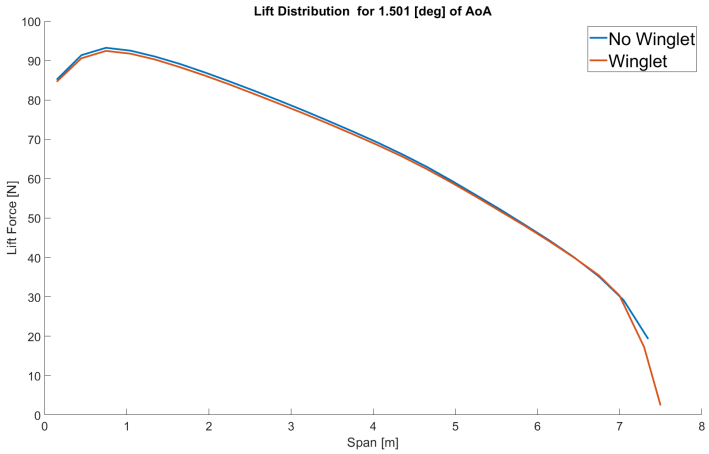

Figure 30: Lift distribution for 95 [kmh] and 1.501 [deg] .

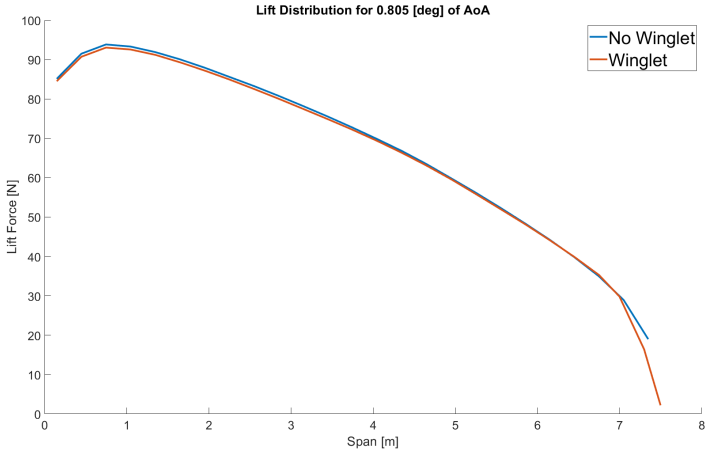

Figure 31: Lift distribution for 100 [kmh] and 0.805 [deg] .

It is possible to see how the Lift force decreases in the last part of the wing, which reduces the pressure differences in the last part of the wing, which is a cause of the decrease of the pressure difference reduction.

4.3 Discussions

As commented in section 4.2.1, an offset of 1 [deg] has been observed in the CL-α graph (figure 22). Even if the flow conditions are not the worse ones for a simulation (incompressible flow) the simulation has been performed in a turbulent transition RANS model, which instead of simulate, models the turbulence. This means that the estimation of the variables done by the software have some uncertainty due to the turbulence model itself. Furthermore the values obtained are in close relation with the ones obtained by Thomas Hansen [1] being the average relation in the steady flight angles of attack of a 13 %. The most important similarity that comes up is the parallelism with the experimental data, which means that the behavior of the aircraft with respect to the reality is reasonable accurate (see figures 23, 24, 25). This leads to a revision of the initial angle of attack used in the simulation. Another possible source of error of the deviation of figure 22 is the method used for the calculation. As a matter of fact only two points are needed for the extraction of a line equation and due to the features of the simulation and also to the nature of the aircraft, the linear behavior is expected, but in order to double check the features of RANS methods more angles of attack could have been evaluated for this matter. Obviously due to the limited time and resources available and given the similarities in the performance together with the deviation of previous studies using the same turbulent models, it can be said that even with the deviations from validation or the uncertainty of the mesh, the simulations have achieved to obtain results close to the reality.

When it comes to talk about estimation of Drag and Drag Coefficients in RANS methods, results of the 2D study have given an idea of the error that can be expected. The overestimation of the drag coefficient despite being non neglectable, it is not a huge deviation and may be caused due to different reasons. The geometry could be slightly different in the model used in comparison with the one used in the experimental data. This could be a source of error which would explain the deviation of the results. On the other hand, it is important to remind that RANS methods do not simulate the reality of the flow evaluated but they model all the turbulence scales, which means that some features of the flow specially in the turbulent regions could be overestimated causing this slight Drag Coefficient overestimation.

The features of the performance of the aircraft shown in figures 24, 25 and table 18 are significantly similar to the experimental data even with the Drag Coefficient overestimation. The values show that the method used is able to predict the behavior of the aircraft with steady flight obtaining results with great similarities to the reality. Despite this accuracy, it has been observed that maximum Aerodynamic efficiency and glide ratio are not located in the experimental speeds which are 96.5 [kmh] and 94.5 [kmh] respectively. In the simulations these maximums are located in 100 [kmh]. In order to verify these measures, additional simulations could be done with the aim of finding this maximum points.

The Oswald factor is a geometric adimensional factor which measures the efficiency of the wing and the aircraft which compares any aircraft with an elliptic

aircraft, which is known because of its good performance with respect to the Induced drag [21]. This happens due to the reduction of pressure difference between the upper and lower surfaces of the wing which reduce the vortex created in the wing tip, cause of the winglet. The Oswald factor is usually calculated by geometrical data, but given the features of the Standard Cirrus Glider wing, which has dihedral angle, sweep angle in the leading and trailing edge and geometrical and aerodynamical twist, it makes the calculations incredibly difficult. The range of action of CFD methods allow to calculate the features of the flow in different conditions and this condition has allowed to calculate an estimation of this parameter. The value obtained from the average of the different cases analyzed gives an Oswald efficiency factor of 0.779 which has a great relation with the typical Oswald factor for gliders which are between 0.8 and 0.9 [19]. The estimation has as basement the assumption of that the Parasitic Drag is only function of the speed and its dependence of the Angle of attack is minimum, which is not exactly true. This assumption is only valid in the steady flight conditions because the angles of attack are fixed to the flight speed. The assumption was considered correct because the difference in angles of attack analyzed in the Oswald Factor calculation is very low. However, it is known that Parasitic Drag is formed by friction and pressure drag, and even if the friction drag is mainly a function of the flight speed, the pressure drag does depend on the angle of attack. The low difference of angle of attack between the cases used in this section was the tool used to calculate this factor. A possible improvement in this section would be the calculation of the drag coefficient for the zero lift condition in the aircraft, which is the definition of the Parasitic Drag. In this way the calculation of the Oswald factor would have been more accurate. Anyway, the estimation method has theoretical background an has demonstrated correlation with the theory due to the lack of experimental data to compare with.

The data shown in table 20 describe the actual changes in the performance of the aircraft, and it is possible to see how the Drag Coefficient decreases an average of 1.5%, which is the desired change when adding a winglet in an aircraft. This difference is higher than the mesh independence uncertainty for CD which is 0.98 %, so it cannot have been produced by the mesh uncertainty. Even with a low value, it is possible to say that the Winglet has achieved its objective. Although the Drag coefficient decreases, it is a minor reduction and this is caused because of the Aspect ratio of the aircraft which is greater than any other type of aircraft. Gliders are known for its aerodynamic efficiency and one of the main reasons is their large aspect ratio which already decreases the Induced Drag. The addition of a winglet in other types of aircraft as airliners report a drag reduction of Drag between 5 and 10% [22]. But due to this large Aspect Ratio, the effect on the drag reduction is lower than it could be in a usual airliner which has an Aspect Ratio around 8.

An interesting fact that is worth to mention is the fact that the pressure drag is reduced in both velocities whereas the friction drag decreases in the 95 [kmh] case, which is not the expected result, given the fact that the winglet adds surface and it should increase the friction forces. The analysis of the specific case relates that the angle of attack of of that velocity creates a low pressure zone in the winglet interior surface and creates an eddy area. This phenomenon detaches the flow from

the winglet surface avoiding the shear stress and reduces it in the final sections of the wing.

The effect of the winglet is clearly visible in 29, where it is possible to see reduction of the low pressure area after the wing tip and the spanwise direction of the air, which is the effect that the winglet runs after.

In the Lift Coefficient analysis and light decrease is found in both cases and this has to do with two reasons. The addition of a winglet results in the cut of 0.1 [m] of wing due to the features of the original wing tip, which reduces the amount of lift force created in the wing. Furthermore, the winglet reduces the lift creation in the last section of the wing due to the winglet sweep angle. The winglet has an stagnation point in the leading edge, and this stagnation point is a source of high pressures which limits the low pressures of the final sections of the wing. This high pressure area extends the winglet effective area and avoids the high pressure located in the lower surface of the wing of going through the wingtip.

Finally figures 30 and 31 show the lift distribution of both geometries and clearly show that the winglet geometry is closely related with the elliptic wing idea due to the lift reduction in the final section of the wing. When including the airfoil, the creation of lift in the last part of the wing is reduced due to the interaction between the winglet and the wing, and the wing reduces the lift creation in the wingtip. This means that the pressure difference at the wingtip will be lower, so the Induced Drag will be reduced, obtaining an elliptical wing distribution which will increase the efficiency of the wing.

4.4 Conclusions

The final conclusions of the 3D study are:

- The model representation of the reality differ in some aspects as the Angle of Attack of the steady flight, but the performance of the aircraft is quite accurate having an averaged error of 6.5%.
- The Oswald Factor Coefficient estimation is very close to the expected value of this type of aircraft.
- The winglets introduced obtain the expected Pressure Drag reduction and the Wing Tip Vortex decreases considerably with respect to the Vortex previously created.
- The Lift reduction differs from the expected results and although the lift distribution gets closer to the elliptic wing distribution, the effective angle of attack has not improved.

5 Perspectives

The present study has shown the possibilities of the model Transition SST in Fluent as well as the methodology followed in this project. During the development of this project some possible extensions have popped up and due to the lack of time have not been possible to carry through. The main extensions are to be done in the 3D part in order to improve the knowledge of the glider.
It has been noticed that the best performance parameters are have not coincided with the experimental ones, but due to the lack of resolution in the study, the actual best performance velocity are unknown. The best extension of the project would be increase the resolution in the speeds analyzed. With this procedure it would be possible to compare the performance of the glider in a more accurate way.
In the Oswald Factor section, as commented in Discussions, an additional simulation per velocity using the zero Lift Angle of Attack would have been very useful to increase the accuracy of the estimation.
In the Winglet section it would be very interesting to analyze the behavior of the winglet used at near Stall Speed with high Angles of Attack as well as a parametric study of different shapes of winglets.

References

[1] Hansen T. Modeling the Performance of the Standard Cirrus Glider using Navier-Stokes CFD. Norwegian University of Science and Technology; 2014. https://www.researchgate.net/publication/286779180_Modeling_the_Performance_of_the_Standard_Cirrus_Glider_using_Navier-Stokes_CFD.

[2] Somers DM. EXPERIMENTAL AND THEORETICAL LOW-SPEED AERODYNAMIC CHARACTERISTICS OF A WORTMANN AIRFOIL AS MANUFACTURED ON A FIBERGLASS SAILPLANE. Langley Research Center; 2014. https://ntrs.nasa.gov/search.jsp?R=19770011105 2019-026T26T16:45:15+00:00Z.

[3] PÃtzold F. Preliminary Results of Flight Performance Determination of Cirrus75 Dâ6607 S/N 633. Institute of Flight Guidance at Technische UniversitÃt Braunschweig; 2012. http://www.deturbulator.org/2011_StdCirrus_D-6607_PreliminaryResults_2013-Jan-06.pdf.

[4] English T. A Look at the history of CFD. The Short Sleeve and Tie Club; 2017. ://shortsleeveandtieclub.com/a-look-at-the-history-of-computational-fluid-dynamics/.

[5] Organization SC. STANDARD CIRRUS. Standard Cirrus Organization; 2012. http://www.standardcirrus.org/Index.php.

[6] Andersson M SJ Nadali N H. Report Formatting for Authors. Division of Applied Thermodynamics and Fluid Mechanics; 2015.

[7] GÃrdhagen R. Lecture notes: Aerodynamics. LinkÃ¶pings Universitet; 2018.

[8] P Marti Gomez-Aldaravi RN. Lecture notes: Ampliacion de Mecanica de fluidos, fluido compresible e incompresible. Universitat Politecnica de Valencia; 2017.

[9] Versteeg MW H K. An introduction to computational fluid dynamics: thefinite volume method. Pearson Education.; 2007.

[10] Menter FR. Two-equation eddy-viscosity turbulence models for engineering applications. AAIA Journal; 1994.

[11] F R Menter SRLYBSPGHSV R B Langtry. A Correlation-Based Transition Model Using Local Variables. Journal of Turbomachinery; 2006. http://www.deturbulator.org/2011_StdCirrus_D-6607_PreliminaryResults_2013-Jan-06.pdf.

[12] John J Bertin RMC. Aerodynamics for Engineers (5th Edition). 5th ed. Pearson Education, Inc.; 2009.

[13] AirfoilTools. Airfoil Tools;. http://airfoiltools.com/plotter/index.

[14] ABBOTT VDAE I H, STIVERS LS. Summary of airfoil data. NACA Technical Report 824; 1945. https://ntrs.nasa.gov/search.jsp?R=19930090976.

[15] M Serdar GenÃ§ HHA Ä°lyas Karasu, Akpolat MT. Low Reynolds Number Flows and Transition. Intech Open; 2012.

[16] Maughmer MD. THE DESIGN OF WINGLETS FOR HIGH-PERFORMANCE SAILPLANES. The Pennsylvania State University; 2003. https://www.researchgate.net/publication/266339609_Design_of_Winglets_for_High-Performance_Sailplanes.

[17] ORG P. Y+ Calculator. PointWise, Inc; 2019. http://www.pointwise.com/yplus/.

[18] Hall N. Downwash Effecths on Lift. NASA, Glenn Research Center; 2015. https://www.grc.nasa.gov/WWW/K-12/airplane/downwash.html.

[19] Sadraey MH. Aircraft Performance: An Engineering Approach. 1st ed. Taylor Francis Group; 2016.

[20] Jr JDA. Introduction to Flight. McGraw Hill; 1989.

[21] Hall N. Induced Drag. NASA; 2015. https://www.grc.nasa.gov/WWW/K-12/airplane/induced.html.

[22] Winglets. NASA, Dryden Flight Research Center; 2014. https://www.nasa.gov/centers/dryden/pdf/89234main_TF-2004-15-DFRC.pdf.

A First appendix

A.1 Location of the Pressure Probes in 3d Mesh Independence

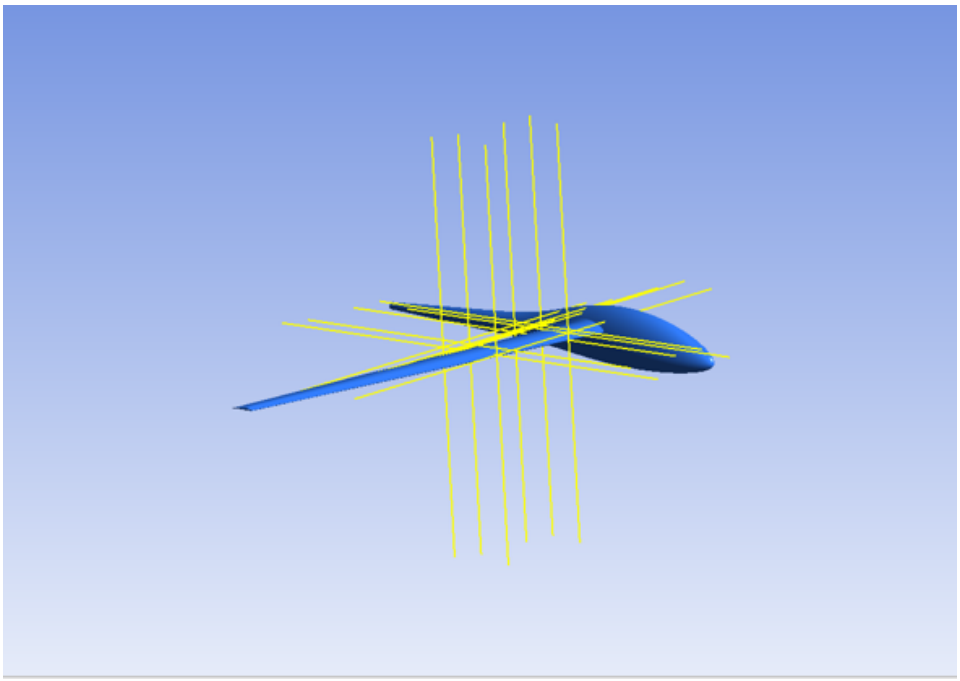

Figure 32: Location of pressure probes of the main body mesh independence

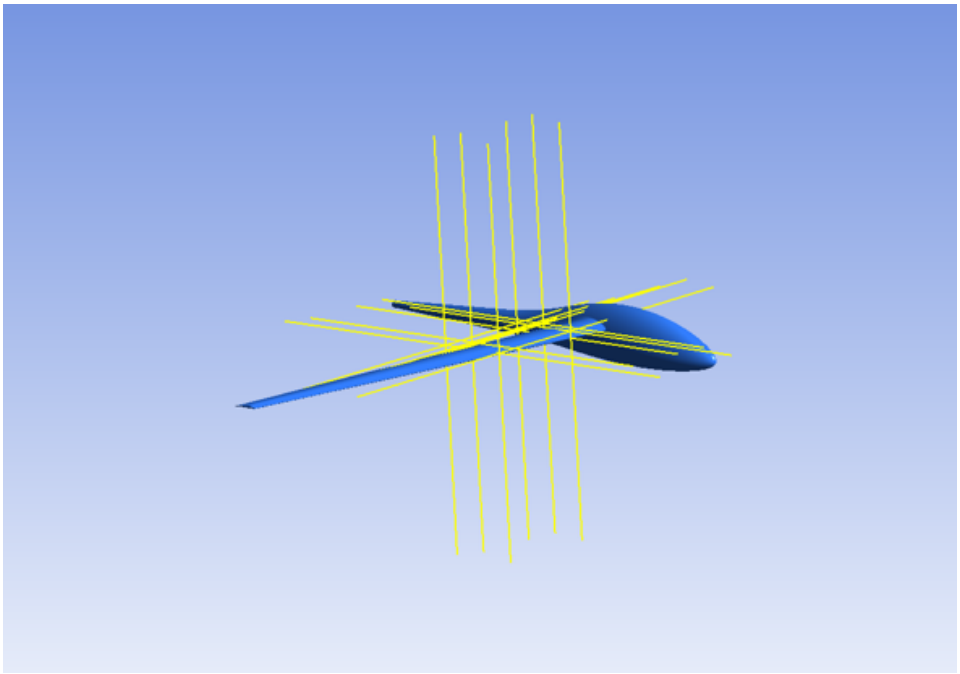

Figure 33: Location of pressure probes of the empennage body mesh independence